Available online at www.sciencedirect.com

SCIENCE DIRECT®

Developmental Biology 267 (2004) 72–92

DEVELOPMENTAL BIOLOGY

www.elsevier.com/locate/ydbio

Frontonasal process-specific disruption of AP-2α results in postnatal midfacial hypoplasia, vascular anomalies, and nasal cavity defects

D.K. Nelson[a] and T. Williams[a,b,*]

[a] *Department of Molecular, Cellular, and Developmental Biology, Yale University, New Haven, CT 06520, USA*

[b] *Department of Craniofacial Biology and Cell and Developmental Biology, University of Colorado Health Sciences Center, Denver, CO 80262, USA*

Received for publication 22 August 2003, revised 23 October 2003, accepted 28 October 2003

Abstract

A majority of the bones of the vertebrate cranial vault and craniofacial complex develop via intramembranous ossification, and are separated by fibrous sutures that undergo osteogenic differentiation in response to growth stimuli. Craniosynostosis is a common human birth defect that results from the premature bony fusion within skull sutures, and causes a myriad of complications including mental retardation and craniofacial anomalies. Synostosis of facial sutures has been reported to cause midfacial hypoplasia in some craniosynostosis cases, but most studies focus on cranial vault sutures. In this study, we have generated a mouse model of frontonasal suture synostosis and midfacial hypoplasia through the tissue-specific elimination of the AP-2α transcription factor. We report here the generation AP-2CRE, a frontonasal process (FNP)- and limb-specific CRE recombinase allele that is directed by human AP-2α promoter and enhancer elements. We used the AP-2CRE line in combination with the conditional AP-2α line to produce a new frontonasal knockout (FKO) mutant that lacks AP-2α in the FNP and limbs. FKO mice exhibit shortened snouts and wide-set eyes that become apparent at postnatal day 15. The most prominent defects in FKO snouts are (1) a lack of growth within the frontonasal sutures, and (2) a reduction in the snout vasculature. Additional defects are observed in the FKO nasal bones and sutures, the nasal cavity cartilage and bony projections, and the olfactory epithelium. The characteristics of the FKO mouse model are a unique combination of midfacial growth anomalies, and provide the first evidence that AP-2α is essential for appropriate postnatal craniofacial morphogenesis.

Keywords: AP-2; Craniofacial; Intramembranous ossification; Suture; Frontonasal; Differentiation; Mouse; Midfacial hypoplasia; CRE recombinase; Interfrontal bone

Introduction

Postnatal craniofacial outgrowth is a dynamic process that requires the coordinated development of several tissues within the vertebrate skull. The craniofacial complex consists of the nasal, premaxillary, and maxillary bones, juxtaposed with the frontal bones of the cranial vault, as seen in a dorsal view of the mouse skull (Fig. 1A). Both the facial and frontal bones are derived from the cranial neural crest (Couly et al., 1992, 1993; Jiang et al., 2002) and undergo intramembranous ossification, and as such are separated by secondary growth sites called sutures. The mesenchyme of the suture junctions is maintained in an undifferentiated state called patency, while the edges of the bones are comprised of nonossified osteoblasts and are called osteogenic fronts or bone fronts. Ultimately, the purpose of patency within the cranial vault sutures is to accommodate the rapid expansion of the brain that occurs after birth. Postnatal membrane bone growth is essentially achieved by the recruitment of suture cells to the osteogenic fronts followed by their differentiation and mineralization, in response to signals from the bone fronts themselves, and the dura mater that overlies the brain (for reviews, see Opperman, 2000; Ornitz and Marie, 2002). Premature ossification of these sutures results in a condition called craniosynostosis, and occurs in approximately 1/2500 live human births (Wilkie and Morriss-Kay, 2001). Such conditions can cause skull deformities, mental retardation, blindness, and facial anomalies because brain expansion continues despite the presence of a defective closed suture.

* Corresponding author. Department of Craniofacial Biology and Cell and Developmental Biology, University of Colorado Health Sciences Center, BRB 151, Campus Box C286, 4200 East Ninth Avenue, Denver, CO 80262. Fax: +1-303-315-3013.

E-mail address: trevor.williams@uchsc.edu (T. Williams).

0012-1606/$ - see front matter © 2003 Elsevier Inc. All rights reserved.
doi:10.1016/j.ydbio.2003.10.033

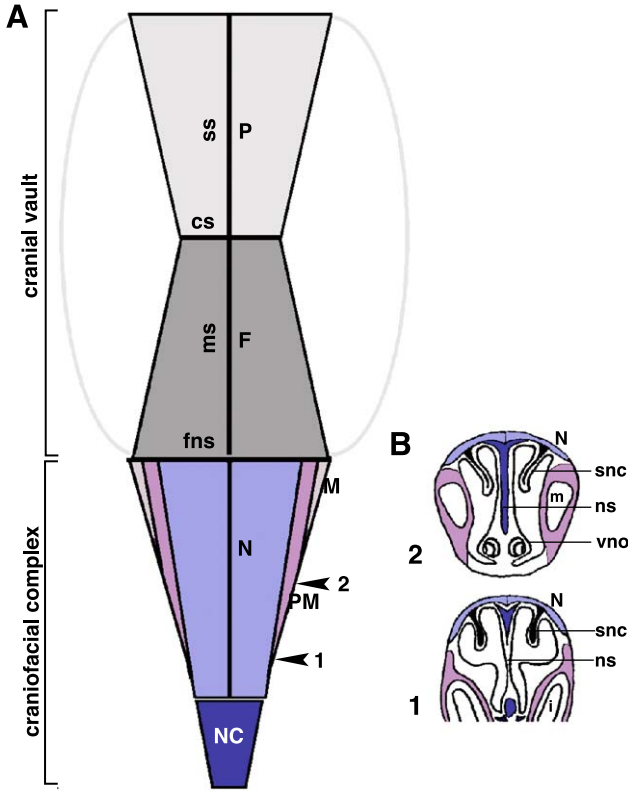

Fig. 1. Schematic representations of postnatal skull components. (A) Dorsal view of skull to illustrate relative positions of bones. Abbreviations: nasal cartilage (NC), nasal bone (N), premaxillary bone (PM), maxillary bone (M), frontal bone (F), parietal bone (P), frontonasal suture (fns), metopic suture (ms), coronal suture (cs), and sagittal suture (ss). (B) Cartoons of coronal sections to illustrate nasal cavity structures. Section 1 is toward distal tip of snout, and section 2 is more proximal to the fns. Additional abbreviations: nasal septum (ns), superior nasal conchae (snc), vomeronasal organ (vno), incisor (i), molar (m). Note: Skull schematic is adapted from Popesko (1992).

Several genes have been associated with particular human craniosynostosis syndromes, and include mutations of FGFR-1 (Pfieffer Syndrome; Muenke et al., 1994), FGFR-2 (Crouzon and Apert Syndromes; Reardon et al., 1994; Wilkie et al., 1995), *TWIST* (Saethre–Chotzen Syndrome; el Ghouzzi et al., 1997; Howard et al., 1997), and MSX2 (Boston-type Craniosynostosis; Jabs et al., 1993).

Proper postnatal facial morphogenesis also requires patency of the facial sutures. In some craniosynostosis cases, premature fusion of facial sutures was reported to inhibit outgrowth of the craniofacial complex, causing a condition called midfacial hypoplasia (Cohen, 2000). Despite their importance, the development of craniofacial sutures is poorly understood. While growth at the osteogenic fronts of the facial bones is similar to that of the cranial vault bones, the facial bones differ in that they overlie the cartilaginous elements of the facial complex rather than the dura mater. In addition, as the nasal and premaxillary bones elongate during the postnatal period, growth at the frontonasal and frontal–premaxillary suture junctions is characterized by interdigitation patterns that become more complex over time.

A majority of genetic and molecular studies focus on the cranial sutures (i.e. coronal and sagittal) because they are usually the most severely affected sites of synostosis in the syndromes described above. Nonetheless, there are several genes that are expressed in the craniofacial complex and may play important roles in facial suture development. For example, FGFR-2 is expressed in the developing bone fronts of both cranial vault and facial bones in late embryogenesis (Iseki et al., 1997). In addition, the expression patterns of TGF-β family members and Msx2 have been characterized within the rat frontonasal suture (Adab et al., 2002), and Msx1 expression was reported in the postnatal mouse frontonasal suture (Orestes-Cardoso et al., 2001). However, aberrant expression patterns of these genes and/or associated signaling processes have not been directly associated with reduced growth at this suture junction.

Internal to the membrane bones of the facial complex are the elements of the nasal cavity. In a coronal (or frontal) view, the nasal cavity is medially bisected by the cartilaginous septum, schematized for the mouse snout in Fig. 1B. Ventral to the nasal bones, the superior nasal conchae project into the cavity, and ultimately give rise to the turbinate bones via endochondral ossification. The vascular mucosa and adjacent epithelial layers line the entirety of the nasal cavity: respiratory epithelia in the distal snout (not shown), and olfactory epithelia in proximal regions (Fig. 1B). In the proximal two-thirds of the cavity, the vomeronasal organ (VNO) is present at the base of the nasal septum, and functions in the chemosensory behaviors of the mouse (i.e. pheromone responsiveness) (Figs. 1B–2) (Wysocki, 1979). Following embryogenesis, it is important that the craniofacial membrane bones and nasal cavity elements develop in a concerted fashion. Through the study of animal models in which these processes are disrupted, we can better understand how the various craniofacial tissues interact for appropriate outgrowth in the postnatal period. In this study, we have generated a facial-specific AP-2α mutant that exhibits postnatal nasal bone and nasal cavity anomalies due to impaired growth within the frontonasal sutures and a reduction in snout vasculature.

AP-2α is the founding member of a small family of transcription factors that are characterized by a C-terminal "basic helix-span-helix" domain required for DNA contact and dimerization (Mitchell et al., 1987; Williams and Tjian, 1991a,b). It is expressed in several tissues throughout embryogenesis including the neural tube, neural crest, facial prominences, and limb bud mesenchyme (Mitchell et al., 1991). Targeted mutagenesis of AP-2α results in a complex and lethal phenotype that includes failure of anterior neural tube closure and severe midfacial hypoplasia (Schorle et al., 1996; Zhang et al., 1996). Chimeric animals composed of wild-type and AP-2α-null cells often exhibit cleft lip with or without cleft palate in the absence of neural tube closure defects, indicating that AP-2α is required for the proper growth and/or fusion of tissues derived from the embryonic frontonasal prominence (FNP) (Nottoli et al., 1998). Inter-

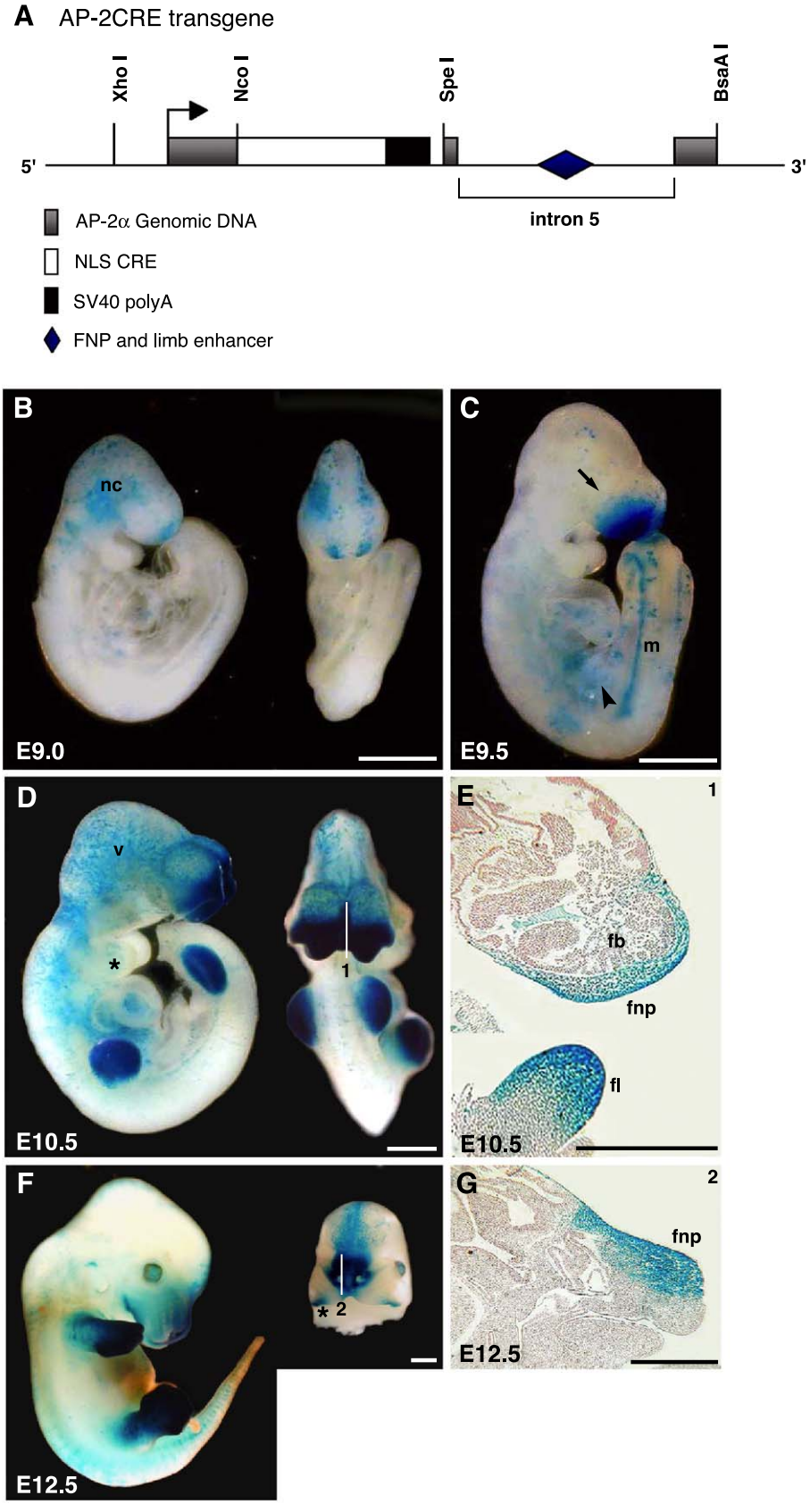
A AP-2CRE transgene
Xho I
Nco I
Spe I
BsaA I
5'
3'
intron 5
AP-2α Genomic DNA
NLS CRE
SV40 polyA
FNP and limb enhancer
B
nc
E9.0
C
m
E9.5
D
v
*
1
E10.5
E
1
fb
fnp
fl
E10.5
F
* 2
E12.5
G
2
fnp
E12.5

estingly, approximately 4% of adult mice in the AP-2α-null/+ colony exhibit a malocclusion due to curvature of the nasal region, which further supports a role for AP-2α in FNP development and suggests that craniofacial tissues are sensitive to reduced levels of the gene (Nottoli et al., 1998). Face and limb development are mechanistically linked (Richman and Tickle, 1989), and many genes perform similar functions in both tissues during embryogenesis (Schneider et al., 1999). In this respect, AP-2α-null mice also exhibit loss of the radius in most mutants, and a percentage of chimeras generated exhibit polydactyly and/or polysyndactyly (Nottoli et al., 1998; Zhang et al., 1996). Taken together, the loss-of-function studies illustrate that functional AP-2α plays important roles in both facial and limb morphogenesis. However, because of the severity of the AP-2α-null neural tube and facial phenotypes, and the variable combinations of face and limb defects that occur in chimeras, it has been difficult to determine the roles of AP-2α in these tissues.

We therefore sought to elucidate the functions of AP-2α in facial and limb development by utilizing the CRE-loxP system of conditional mutagenesis. The first component of this system is the conditional allele of AP-2α (Alflox) that was recently generated in our laboratory (Brewer et al., 2003). The Alflox allele contains loxP sites that flank exons 5 and 6, which encode a portion of the helix-span-helix domain that is essential for AP-2α function. To target the face and limbs, we report here the generation and characterization of the second component: a novel transgenic line (AP-2CRE) in which CRE recombinase expression is driven by an FNP- and limb-specific enhancer element, derived from the human AP-2α gene (Zhang and Williams, 2003). Crossing Alflox and AP-2CRE lines of mice results in the elimination of AP-2α from the embryonic face and limb mesenchyme. These conditional FKO (FNP knockout) mutants exhibit postnatal facial shortening that becomes apparent approximately 15 days after birth, and they do not display overt limb abnormalities. We have characterized the progress of the FKO phenotypes as the mice mature, and have identified defects within a subset of facial sutures, as well as the nasal bones, the snout vasculature, and skeletal elements of the nasal cavity. Previous studies have indicated that AP-2α is expressed in the mesenchyme of the embryonic facial primordia. We report here that this gene is also expressed in postnatal facial tissues. Therefore, the absence of functional AP-2α from FKO craniofacial tissues in both pre- and postnatal periods likely contributes to the observed phenotypes. In conclusion, the combination of defects found in FKO mice represent a unique mouse model of midfacial hypoplasia, and this study provides the first evidence that functional AP-2α is directly required for appropriate postnatal craniofacial morphogenesis.

Materials and methods

Mouse strains and PCR genotyping

The AP-2CRE transgenic construct was made by first cloning a 200 bp *Xho*I–*Nco*I fragment of the human AP-2α promoter into pBluescript. The NLS Cre (gift from Gail Martin) was introduced using *Nco*I and *Eco*RV restriction sites. A SV40 poly-A tail was then cloned in downstream of the NLS CRE using *Eco*RV and *Bam*HI restriction sites. To generate AP-2CRE, a 1.8-kb enhancer element from human AP-2α, spanning the middle of exon 5 through the middle of exon 6 was introduced downstream of the poly-A tail. The AP-2CRE plasmid DNA was prepared with the Qiagen MaxiPrep kit, linearized, and purified for injection at the Yale University Transgenic Core Facility. AP-2CRE genotyping was accomplished by PCR amplification of a 350-bp fragment spanning the AP-2α promoter and CRE sequences. Primer sequences were: CRE4 5′-GCG CTA ACC CAG AGA GTA GCT CC-3′ and CRE5 5′-CGC GAA CAT CTT CAG GTT CTG CGG G-3′. The generation of the conditional Alflox line will be described elsewhere (Brewer et al., 2003). The primers Alflox4, 5′-CCC AAA GTG CCT GGG CTG AAT TGA C-3′ and Alfscsq 5′-GAA TCT AGC TTG GAG GCT TAT GTC-3′ were used for genotyping, and generate a 490-bp fragment from the wild-type AP-2α allele, and a 560-bp fragment from the Alflox allele. The AP-2α-null/+ line was described in Zhang et al. (1996), and the primers Alpha 3′KO 5′-CGT GTG GCT GTT GGG GTT GTT GCT GAG GTA C-3′ and neo 3′ KO 5′-AAC GCA CGG GTG TTG GGT CGT TTG TTC G-3′ were used for genotyping.

Breeding AP-2CRE/AP-2α-null/+ males with Alflox heterozygous or homozygous females generated the FKO line of mice. To genotype FKO offspring, DNA was isolated from tail biopsies of all pups between P1 and P15 using the DNeasy kit (Qiagen), and 5 μl was then used in the PCR reactions. Tail tissue DNA from embryos was directly prepared in a one-step lysis buffer as described for yolk

Fig. 2. Characterization of AP-2CRE transgene activity in mid-embryogenesis using the R26R reporter strain. (A) Schematic representation of AP-2CRE transgene that contains the human AP-2α promoter and intron 5 frontonasal prominence (FNP) and limb enhancer elements. In whole-mount β-galactosidase assays, AP-2CRE activity begins in the cranial neural crest cells (nc) in the lateral regions of the head at approximately (B) E9.0. (C) At E9.5, activity is strong in the FNP, mesonephros (m), and is faint the forelimb buds (arrowhead). The arrow indicates the migratory path of cranial neural crest cells. (D) By E10.5, activity is strong in both FNP and limb bud mesenchyme. Vascular tissue (v) in the head and a small portion of the first branchial arch (*) are also positive. (E) A majority of distal cells are AP-2CRE positive in sections through the middle region of the FNP (upper) and forelimb bud (lower). (F) At E12.5, CRE activity is most robust around nasal pits in the center of the face, as seen in a sagittal section through FNP (G), as well as in the distal regions of fore- and hindlimbs (F). Note: Numbered lines in D and F designate planes of sections in E and G, respectively, and fb indicates the forebrain in E (top). Size bars represent 1.0 mm.

sac genotyping (Solloway and Robertson, 1999), and 3 μl was used in PCR reactions. All offspring were genotyped with primer sets described above for AP-2CRE, AP-2α-null, and Alflox alleles.

Probe generation and in situ hybridization

To generate the AP-2e6 ISH probe, total RNA was isolated from microdissected wild-type branchial arch 1 samples using the RNeasy kit (Qiagen). Total RNA, 0.5 μg, was used to generate first-strand cDNA with the First-strand Synthesis kit (Amersham). The AP-2e6 ISH fragment was amplified from the cDNA by PCR, and corresponds to exon 6 of the mouse AP-2α gene (gi 6755733, nucleotides 954–1087). The primers were AP-2EX6A, 5′-GAG AAG CCG TCC ACC TAG CC-3′ and AP-2EX6B, 5′-GCA GAT CTG TTT TGT GGC CAG-3′. The amplified DNA was directly cloned into the pPCR-II plasmid with the Topo TA Cloning kit (Invitrogen). Positive clones were identified by digestion with *Eco*RI and sequenced at the HHMI Keck Core Facility at Yale University.

For whole-mount ISH, the AP-2e6 probes were generated according to Riddle et al. (1993), using 11-digoxigenin (DIG)-UTP (Roche). For the sense control probe, the AP-2e6 plasmid was linearized with *Not*I (New England Biolabs-NEB) and transcribed with SP6 RNA polymerase (NEB). For the antisense probe, the AP-2e6 plasmid was linearized with *Bam*HI (NEB) and transcribed with T7 RNA polymerase (Roche). After synthesis, RNA probes were precipitated and resuspended in 50 μl diethyl pyrocarbonate (DEPC)-treated water (DEPC, Sigma). Note that the sense control probe does not detect specific expression at E10.5 (data not shown). The FGFR-2 probe was a generous gift from J. Rossant, and was generated as previously described (Ciruna and Rossant, 1999).

Noon on the day of the copulatory plug was considered to be embryonic day (E) 0.5. For whole-mount ISH, embryos were taken at E10.5 (AP-2e6) and E17.5 (FGFR-2) and dissected in DEPC-treated, ice-cold phosphate-buffered saline (PBS) pH 7.4–7.6. Samples were fixed overnight in 4% paraformaldehyde (PFA; Sigma) in DEPC-PBS, and were processed as previously described (Wilkinson, 1992), with minor modifications. For E10.5 embryos, proteinase K digestion was 15 min, and overnight hybridization was performed in 1 ml of hybridization solution to which 2 μl of DIG-labeled AP-2e6 probe was added. For E17.5 skulls, proteinase K digestion was performed for 45 min, and hybridizations were performed in 1 ml of hybridization solution to which 3 μl of DIG-labeled FGFR-2 probe was added. Alkaline phosphatase conjugated antidigoxigenin antibody (Roche) was used at a dilution of 1:1000 overnight at 4°C and detected with BM Purple substrate (Roche). The reaction was monitored between 1 and 4 h until the color developed, and the embryos and skulls were subsequently washed in three changes of PBT. To intensify the color reaction, specimens were dehydrated and immediately rehydrated through a graded methanol series in PBT. When necessary, embryos were cleared in PBT:Glycerol (1:1, Sigma).

Whole-mount β-galactosidase assays

Embryos were harvested and dissected in PBS. To assay skull and limb samples, the epidermis was removed from the heads and limbs of E15.5 and E17.5 embryos and all postnatal specimens. β-galactosidase assays were performed as previously described (Hogan et al., 1994). Briefly, all specimens were lightly fixed in 0.25% glutaraldehyde (Sigma) for 30 min and incubated in Xgal substrate (Denville Scientific) solution for 1–2 h for AP-2CRE/R26R, or 2–4 h for AP-2KI. To avoid the limitation of Xgal penetration, specimens were cut into pieces, stained, and processed for paraffin sectioning. Skulls were bisected in the coronal or sagittal plane to allow for staining of the nasal cavities, while limbs were cut in the transverse plane.

Skeletal preparation and staining

Skeletal preparations were performed as previously described with minor modifications (Hogan et al., 1994). Briefly, samples were fixed and dehydrated in 95% ethanol for a minimum of 3 days, transferred to alcian blue for 24 h, rinsed in three changes of 95% ethanol, and soaked in 95% ethanol overnight. Samples were subsequently cleared in 1% potassium hydroxide (KOH) for 30 min to 2 h, and stained in alizarin red for 1–3 h. Samples were rinsed in 2% KOH until they were clear, transferred to 20% glycerol in KOH overnight, and stored in glycerol:100% ethanol (1:4).

Tissue preparation and paraffin processing

Embryos between E9.0 and E17.5 were harvested and fixed overnight in 4% paraformaldehyde (PFA) in PBS at 4°C, rinsed in PBS, dehydrated through a graded ethanol series in PBS, and cleared in xylene as previously described (Hogan et al., 1994). For paraffin embedding, Paraplast (VWR Scientific) was melted at 62°C and samples were introduced to xylene:Paraplast (1:1) for 30 min, followed by one change of paraffin for 30 min, and then placed into fresh paraffin overnight.

Postnatal skulls were either decalcified overnight (rapidly) with CalEx (Fisher Scientific) according to manufacturer's instructions, or slowly with 10% EDTA/0.2% PFA made in PBS, pH 8.0 (samples were stored at 4°C, and the solution was changed every 3–4 days for 2–6 weeks). After either decalcification procedure, samples were rinsed in running water for 3 h, transferred to 70% ethanol, and embedded in paraffin in an automated processor.

All paraffin sections were cut on a Microm HM340 microtome: 6 μm for E17.5 through P5 samples, and 8–10 μm for P10 and P15 specimens. For all procedures, slides

were warmed at 60°C for a minimum of 60 min, dewaxed in two changes of xylene, and rehydrated through an ethanol series to water or PBS depending on the procedure. Hematoxylin and eosin (H&E) staining was performed with working solutions obtained from Poly Scientific according to manufacturer's instructions. Alcian blue staining was performed as previously described (Bancroft and Stevens, 1982) and slides were counterstained with nuclear fast red. After staining, slides were dehydrated and coverslipped using Permount (Fisher Scientific).

Plastic embedding, sectioning, and staining

Samples between P10 and P21 were skinned and fixed in 10% neutral buffered formalin for 4 h, washed in PBS, and transferred to 70% acetone. All subsequent steps were performed at the Yale University Core Center for Musculoskeletal Disorders, according to the rapid embedding method described in Kacena et al. (2003). Briefly, samples were transferred into 70% ethanol, dehydrated through graded ethanol series, and infiltrated with destabilized methyl methacrylate (Sigma) solution at 4°C under a vacuum for 3 days. Samples were then transferred to catalyzed methyl methacrylate, and placed at 37°C for 2 days. Glass vials were removed from heat and stored at −20°C. Blocks were then trimmed and sanded and 4-μm sections were obtained with a Leica 2165 Microtome and a tungsten carbide knife, D-profile. Sections were placed on silane-plus coated slides (Scientific Device Laboratories) and incubated at 60° overnight. Slides were then processed though toluidine blue or Von Kossa staining according to standard procedures (Recker, 1983).

Proliferation assays

To detect proliferation in skulls, pups were injected with 100 μg/g of body weight bromodeoxyuridine (BrDU, Roche) in sterile PBS (Miller and Nowakowski, 1988). The mice were sacrificed 2 h after injection and the skulls were fixed overnight in 4% PFA in PBS at 4°C, slowly decalcified, processed through paraffin, and cut at 6 μm. Slides were processed for the BrDU detection procedure essentially as described by Morgenbesser et al. (1995). To detect the BrDU, mouse anti-BrDU antibody (Roche) diluted 1:100 was used with the avidin/biotin blocking kit (Vector Laboratories), the MOM kit (Vector Laboratories), and the DAB kit (Vector Laboratories), according to manufacturer's instructions. For PCNA detection, immunohistochemistry was performed with the mouse NCL-L-PCNA antibody (Vector Laboratories), in combination with the kits described above for the BrDU procedure. A 1:100 dilution of the anti-PCNA antibody was used at 4°C overnight. Control slides containing no anti-BrDU or anti-PCNA antibody did not have appreciable levels of background stain (data not shown).

Statistical analyses

P values for measurements and cell counts were calculated with the Student's *t* test of probability. The external measurements of snout length and interorbital distance were obtained from 10 wild-type and 6 mutant samples, and the *P* value was obtained with the following parameters: two-sample equal variance and two-tailed distribution. P30 skull measurements and BrDU cell counts were performed on equal numbers of samples so paired and two-tailed analyses were performed.

Results

AP-2CRE activity is confined to the FNP and distal limb bud

AP-2α expression in the embryonic FNP and limb bud mesenchyme is directed, in part, by an element in the fifth intron of the AP-2α gene that was identified in transgenic enhancer mapping studies (Zhang and Williams, 2003). We took advantage of these findings to generate the AP-2CRE transgene, which is composed of 0.2 kb of the human AP-2α promoter, encompassing the 5′ UTR. The promoter sequence is fused in frame to the CRE recombinase gene, which contains a nuclear localization signal (NLS-CRE), followed by a 1.8-kb fragment of human AP-2α that spans intron 5 (Fig. 2A). Two independent AP-2CRE transgenic lines were generated, and the recombinase activities were characterized by breeding founder males and subsequent positive male offspring with female R26R reporter mice (Soriano, 1999). We then analyzed the activation of the floxed *lacZ* gene in AP-2CRE/R26R embryos by performing whole-mount β-galactosidase assays. Offspring from the two AP-2CRE lines had identical characteristics (Fig. 2 and data not shown).

AP-2CRE expression begins between E8.75 and E9.0 in lateral head mesenchyme and migrating cranial neural crest cells (Fig. 2B). At E9.5, β-galactosidase activity is now strong in the FNP but it is minimal in the lateral regions of the head, which reflects the migratory properties of the cranial neural crest (compare Fig. 2B with Fig. 2C). In addition, mesonephric tissues are positive at this stage and activity is just beginning in the limb bud mesenchyme (Fig. 2C). By E10.5, distinct medial and lateral nasal prominences (MNP and LNP, respectively) have arisen from the FNP, and expression associated with the head at this stage is strongest in these MNP and LNP tissues. There is also a small positive region within the first branchial arch and variable levels of β-galactosidase activities are present within the vascular network of the head (Fig. 2D). In sections from E10.5 samples, most of the mesenchymal cells in the MNP and LNP are positive, and patchy activity is observed in the overlying facial ectoderm (Fig. 2E and data not shown). With respect to the E10.5 limb buds, β-galactosidase

activity is most robust in the distal mesenchyme, encompassing the cells within the presumptive progress zone (Fig. 2E). Note that the domains of AP-2CRE-mediated activity in the face and limbs represent a specific subset of the tissues in which the endogenous AP-2α gene is expressed (Mitchell et al., 1991).

Between E10.5 and E12.5, the craniofacial complex undergoes several significant changes, including outgrowth and fusion of the facial prominences. β-galactosidase activity in E12.5 AP-2CRE/R26R embryos reflects these morphogenetic processes, highlighting how the FNP tissues give rise to the most central features of the developing face (Fig. 2F, right) including the area surrounding the nasal pits and the medial portion of the upper lip. In addition, there is a small region of positive cells in the ventral maxillary prominence, but otherwise the AP-2α enhancer element we used does not drive expression in the branchial arches (Fig. 2F, right; Zhang and Williams, 2003). In the limb bud, β-galactosidase activity is strongest in the handplate and is less robust toward the proximal regions of the limbs (Fig. 2F, left). Similar to E10.5 embryos, sections through the FNP and limb buds at E12.5 show that most of the distal mesenchyme cells are positive (Fig. 2G and data not shown). In stages beyond E12.5, β-galactosidase activity remains confined to the derivatives of the FNP and distal limb bud mesenchyme (see below; data not shown).

AP-2CRE/R26R marks FNP and distal limb derivatives

To determine the structures to which AP-2CRE-positive cells ultimately contribute, we utilized the lineage tracing properties of the R26R line and performed β-galactosidase assays with AP-2CRE/R26R mice at late embryonic and postnatal time points. Whole-mount skull preparations between E15.5 and postnatal day (P) 15 reveal that AP-2CRE activity marks the precursors of the following tissues: the nasal bones and nasal sutures, the frontonasal sutures, a small portion of the frontal bones, and the metopic suture (Figs. 3A,B). Also, small regions of the premaxillary bones are positive at P15 (Fig. 3B). In sections obtained from P1 embryos, robust activity is found in the nasal bones and sutures, the cartilage throughout the nasal cavity, and the nasal mucosa lining the cavity (Figs. 3C,D). It is noteworthy that β-galactosidase activity is not found in the posterior regions of the frontal bones, the frontal-premaxillary sutures, or within the blood vessels of the nasal cavity.

To address AP-2CRE activity in forelimb derivatives, whole-mount β-galactosidase assays were performed with a series of limbs from which the outer tissues were removed to expose the inner layers of skeletal muscle and bone. AP-2CRE activity is not found in the ectoderm (Fig. 3) and the *lacZ* substrate does not penetrate the epidermis beyond E15.5 (data not shown) and therefore all whole-mount samples from later timepoints were stained following removal of the skin. At E17.5 and P1, β-galactosidase activity was present from the tips of the digits to the middle portion of the skeletal muscle that surrounds the humerus (data not shown). Similarly, at P5, AP-2CRE/R26R-mediated β-galactosidase activity was most robust in the distal limb elements, in both the skeletal muscle and tendons of the zeugopod (Fig. 3E). Further, limb bones stained after the removal of the skeletal muscle exhibited robust activity along the ulna and radius, while patchy activity was observed in the humerus (data not shown). Next, sections of AP-2CRE/R26R forelimbs were analyzed for β-galactosidase activity between E15.5 and E17.5. This analysis demonstrated that the distal mesenchyme cells were uniformly targeted by the AP-2CRE transgene, including the skeletal condensations of the digits, radius, and ulna (Figs. 3F,G) and the skeletal muscle (data not shown). Together, the data indicate that AP-2CRE-mediated β-galactosidase activity is greatest within the distal limb derivatives.

AP-2α is successfully eliminated from the developing FNP and limb buds using AP-2CRE

We next tested the AP-2CRE transgene in the context of the conditional AP-2α allele (Alflox) (Brewer et al., 2003), and accomplished this tissue-specific disruption in a two-step breeding scheme. First, male mice positive for AP-2CRE were crossed with AP-2α-null/+ females. Males containing the AP-2CRE::AP-2α-null/+ combination were then bred with Alflox heterozygous or homozygous females, and the offspring were examined for craniofacial and/or limb defects. Facial anomalies were only observed in progeny with the combination of AP-2CRE::Alflox::AP-2α-null alleles, and are called FKO for "FNP-Knockout" mice.

To confirm the loss of AP-2α from the embryonic FNP and limb buds in FKO mice, in situ hybridization (ISH) was performed using a 144-nucleotide RNA probe specific for the sixth exon (AP-2e6). Exon 6 is present in the wild-type AP-2α and the nonrecombined Alflox alleles, and it is absent from the AP-2α null and the recombined Alflox alleles. Whole-mount ISH with the AP 2e6 probe was carried out at E10.5 on embryos of all genetic combinations. In wild-type embryos, the FNP, branchial arches, limb buds, and the neural tube are all positive for AP 2e6 (Figs. 4A–C). In FKO embryos, AP-2α is not expressed in the FNP and limb buds, while the neural tube pattern is similar to that of wild-type littermates (Figs. 4D–F) demonstrating that AP-2α is deleted only from the appropriate tissues in the FKO combination.

FKO mice exhibit postnatal craniofacial anomalies

FKO embryos examined at E12.5 and E15.5 did not display any morphological defects (data not shown). Several litters were allowed to mature, and at weaning we found that all FKO mice had shortened, more rounded snouts and subtle interorbital hypertelorism relative to wild-type littermates (see Fig. 5).

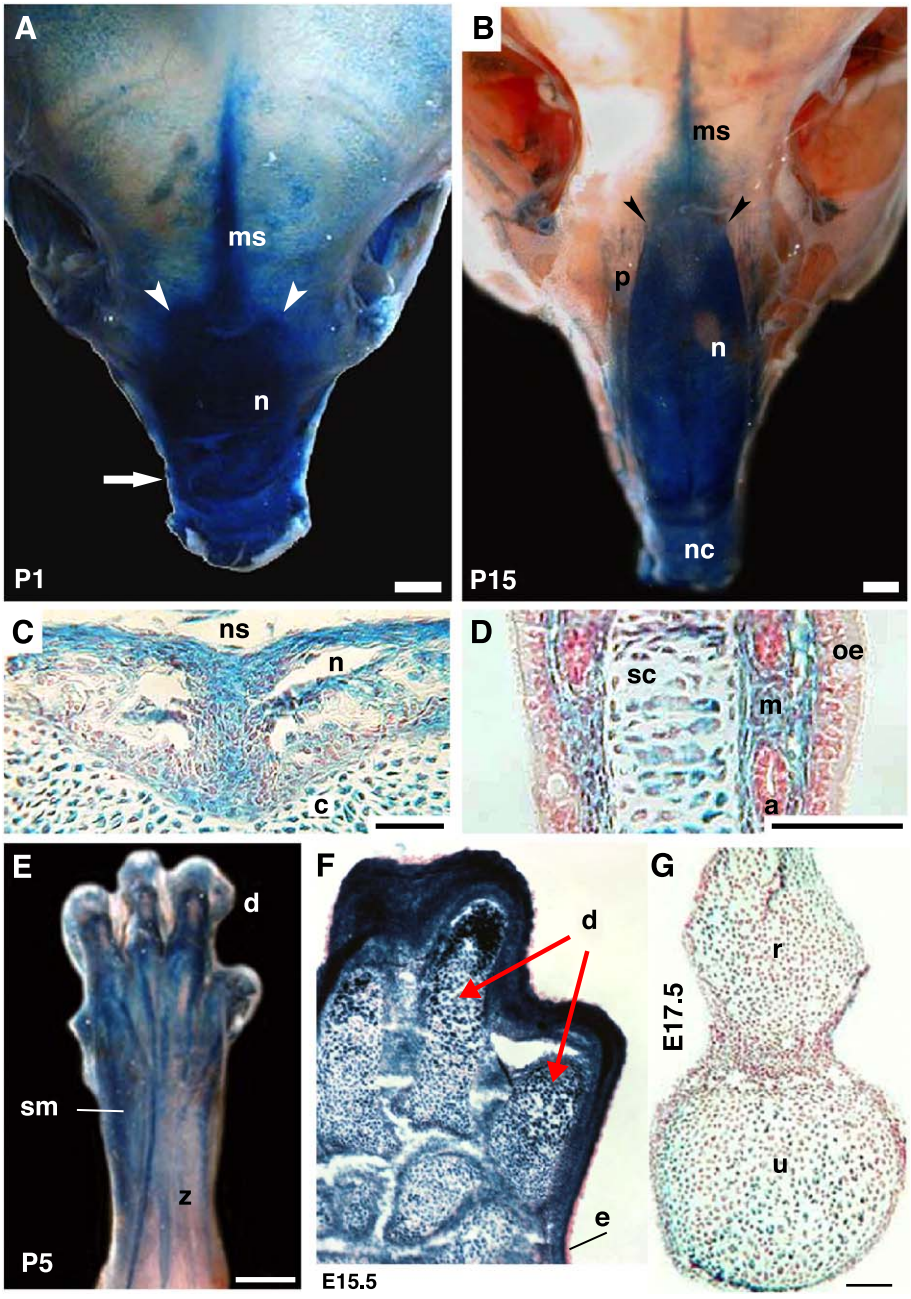

Fig. 3. AP-2CRE transgene activity in skull and limb derivatives. Whole-mount β-galactosidase assays of AP-2CRE/R26R positive skulls at P1 (A) and P15 (B) show strong activity is present in nasal bones (n) and suture, the nasal cartilage (nc), the frontonasal suture (arrowheads), and the metopic suture (ms). In serial sections at P1 (at the level of the arrow in A), AP-2CRE mediated β-galactosidase activity is robust in (C) the nasal bones and suture (ns), and (D) the septal cartilage (sc), and nasal cavity mucosa (m). Activity is not present in the olfactory epithelia (oe), or mucosal arteries (a). (E) In skinned P5 limbs, the distal two-thirds of the zeugopod (z) is positive, including digits (d) and skeletal muscle (sm). (F) Sagittal section through the handplate at E15.5 to illustrate AP-2CRE-mediated β-galactosidase activity is present throughout the mesenchyme, including cells that give rise to the skeletal condensations of the digits (d). Note that the overlying ectoderm (e) lacks β-galactosidase activity. (G) AP-2CRE activity has also targeted the cells giving rise to the radius (r) and ulna (u). Size bars represent 1.0 mm.

Litters were then examined at various postnatal stages beginning at P1 to determine when facial defects become apparent. As late as P10, there are no obvious external differences between wild-type and FKO pups (Fig. 5A). By P15, FKO mice can be distinguished from wild-type littermates because the tips of their snouts are slightly flattened (data not shown). At P21 and later stages, 100% of mutants are readily identifiable due to visibly shorter snout lengths and slightly wide-set eyes (Fig. 5B and data not shown). External measurements have been obtained from the ears to the tip of the nose and between the eyes for mice at P30. The FKO snouts (n = 5) at this time point were approxi-

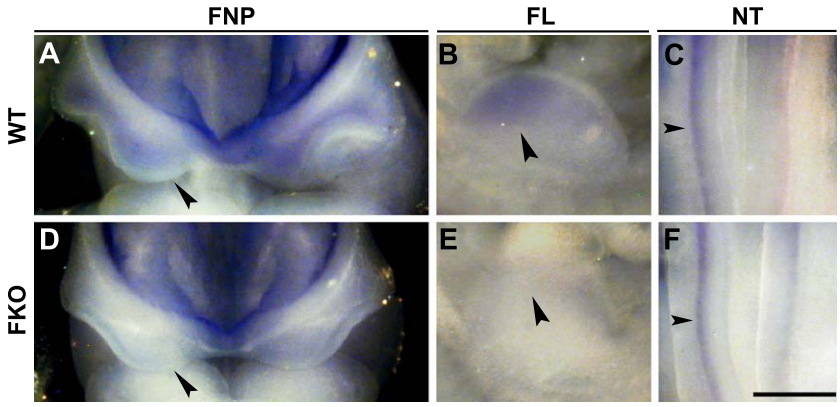

Fig. 4. AP-2e6 ISH expression patterns at E10.5. (A,D) Frontal view of frontonasal prominence (FNP). (B,E) Lateral view of forelimb (FL). (C,F) Dorsal view of neural tube (NT). In wild-type (WT) embryos, AP-2e6 expression is present in (A) FNP, (B) FL, and (C) NT. In FKO embryos, expression is absent from (D) the FNP and (E) FL, but remains in (F) the NT. Note: Intense stain in brain tissues (A,D) is due to trapped probe, and is not specific to AP-2α expression. Size bar (F) represents 0.5 mm, same scale for A–F.

mately 14% shorter, and the eyes were set approximately 11% wider than those of wild-type ($n = 10$) littermates ($P < 0.005$ and $P < 0.001$, respectively). Such differences correspond to a 1–2 mm difference in each dimension. Importantly, the overall body lengths from the base of the tail to the base of the skull were similar between all mice measured (6.5–7.0 cm), indicating the defects in the FKO mice are specific to the snout.

Skull preparations reveal nasal bone and suture defects in FKO snouts

To determine which craniofacial elements are affected in FKO pups, skull preparations at several late embryonic and postnatal stages were stained with alcian blue and alizarin red to visualize cartilage and bone, respectively. From E15.5 through P5, wild-type and FKO skulls show similar patterns of craniofacial cartilage and bone staining, indicating that early skeletal development is not impaired in the mutants (Figs. 5C,D and data not shown). However, by P10, the FKO nasal bones are visibly shorter than in matched wild-type samples, and the lengths of the mutant facial skeletons are slightly reduced (Figs. 5E,F), despite the observation that the pups do not exhibit obvious external differences (see Fig. 5A).

As postnatal outgrowth continues, the elements of the mutant facial skeleton become more severely affected. We compared wild-type and FKO samples by aligning them at the coronal sutures, as skull structures caudal to the frontal bones are neither targeted by AP-2CRE nor affected in FKO mice. At P15 and later stages, the FKO snouts are obviously shorter than in wild-type samples and the nasal bones are truncated, indicating that both bone and cartilage outgrowth are reduced in the mutants (Figs. 5G,H and data not shown). P30 skulls ($n = 4$) were prepared and several differences were found between the wild-type and FKO nasal regions. Measurements taken from the coronal suture to the tip of the nasal cartilage reveal that the mutant snouts are approximately 14% shorter than those of wild-type littermates at this stage ($P < 0.05$), and the FKO nasal bones themselves are approximately 18% shorter ($P < 0.05$). Of interest, due to the nasal bone truncation, the distal nasal cartilage appears longer in FKO samples when compared to wild-type counterparts (Figs. 5G,H). Furthermore, the mutant nasal bones are squared at the ends, in contrast to the tapered wild-type bones (Figs. 5G,H and K,L). In lateral views of P30 snouts, wild-type samples are convex and the distal edges of the nasal bones are in line with the distal edges of the premaxillary bones (Fig. 5I). In contrast, the FKO samples tend to be concave, and it is clear that mutant premaxillary bones extend beyond the distal edges of the nasal bones (Fig. 5J). This altered arrangement of the FKO facial bones results in an anterior shift of the upper incisors toward the distal nasal cartilage, as compared to wild-type samples (Figs. 5I,J). Further examination of the skeletal preparations revealed that in addition to the nasal bone defects, the FKO frontal bones are approximately 13% shorter ($P < 0.05$) and the FKO interorbital distances are approximately 5% wider ($P = 0.05$) than those of wild-type littermates (Figs. 5G,H and data not shown). The nasal and frontal bones approximate between the orbits at the fronto-nasal sutures, and two major defects are apparent in this junction in mutant skull preparations. First, the mutant frontonasal sutures are displaced posteriorly with respect to the frontal–premaxillary sutures (Figs. 5K,L). Second, the FKO frontonasal sutures do not exhibit the extensive interdigitation patterns observed in wild-type littermates. It is important to note that both wild-type and FKO frontal-premaxillary sutures, structures that are not targeted by AP-2CRE, have similar degrees of interdigitation (Figs. 5K,L, asterisk).

Finally, another defect we observed in FKO mice was the presence of ectopic bone within the metopic sutures, called interfrontal (IF) bone. One hundred percent ($n = 20$) of late embryonic and early postnatal FKO skull preparations exhibited some degree of IF bone, ranging from a small

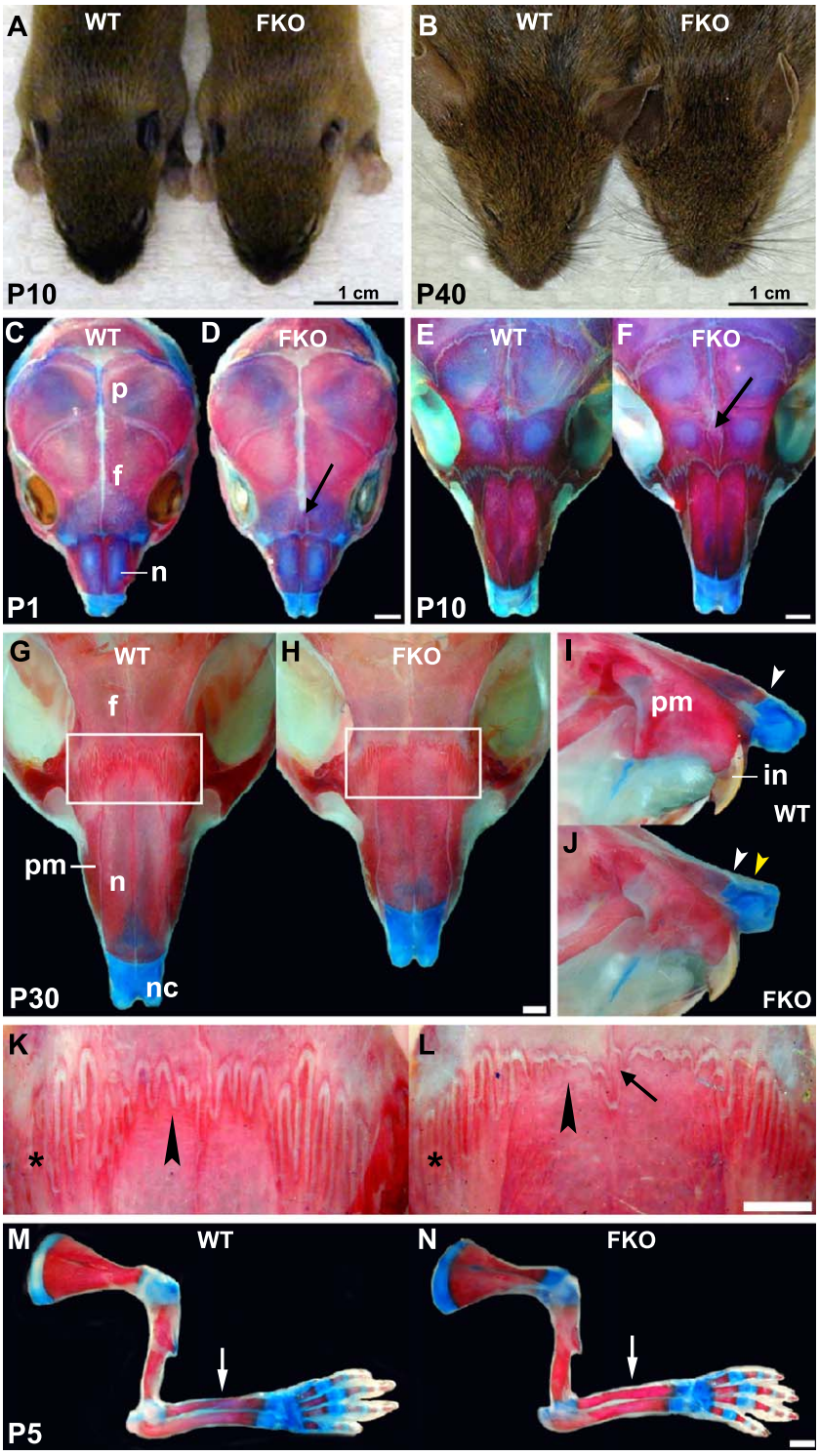

Fig. 5. Postnatal craniofacial defects in FKO mice. (A) At P10, wild-type (WT; left) and mutant (FKO; right) pups have similar external facial morphologies. (B) At P40, FKO mice (right) exhibit shortened snouts and interorbital hypertelorism. (C–N) Skeletal preparations stained with alcian blue (blue) and alizarin red (red) to visualize cartilage and bone, respectively. (C,D) At P1, WT FKO snouts are similar in size and shape. (E,F) At P10, snout and nasal bones from a WT are slightly longer than in an FKO mutant. (G,H) At P30, the FKO snout is approximately 2 mm shorter than wild type. Lateral views of P30 snouts show that in a WT sample (I), the distal edges of the nasal and premaxillary bones are in line (arrowhead). In contrast, (J) the distal edge of the FKO nasal bone (white arrowhead) is visibly shorter than that of the premaxillary bone (yellow arrowhead). (K) WT frontonasal (arrowhead) and frontal–premaxillary (*) sutures are interdigitated. In contrast, the FKO frontonasal sutures (L) lack interdigitation, but the frontal–premaxillary suture is similar to WT. (M) WT and (N) FKO limbs are similar. Abbreviations: frontal bone (f), premaxillary bone (pm), nasal bone (n), nasal cartilage (nc), incisor (in). Arrows in panels D, F, and L mark the interfrontal bone. Size bars (C–N) represent 1.0 mm.

sliver (Fig. 5L) to an obvious wedge between the distal third of the frontal bones (Figs. 5D,F; also see Fig. 9B). Note that IF bone was also found in 44% (n= 60) of the skulls of all other genetic combinations that resulted from our breeding scheme, including embryos that did not contain any of the genetically manipulated AP-2α alleles (data not shown). Thus, the deletion of AP-2α in the FKO mice significantly increases the incidence of IF bone.

FKO forelimbs do not have obvious defects

AP-2α is expressed in the progress zone of the limb bud, and the forelimbs of mice lacking AP-2α frequently show defects in the zeugopod or autopod (Nottoli et al., 1998; Zhang et al., 1996). To determine if the loss of AP-2α from the distal limb mesenchyme in FKO mutants affected limb morphology, wild-type and FKO limbs were prepared and stained to visualize bone and cartilage. Unlike the distal forelimb defects found in previous AP-2α mutant studies, no obvious morphological differences were observed in the mutant fore- or hindlimbs at any of the embryonic or postnatal stages examined (Figs. 5M,N and data not shown).

Loss of AP-2α from the embryonic FNP results in frontonasal suture defects

Histological analyses were performed in sectioned materials to determine the extent to which the nasal and frontal bones, and the associated frontonasal sutures, were affected in the FKO snouts. Decalcified, paraffin-embedded samples were stained with hematoxylin and eosin (H&E) for structural analyses. Within the frontonasal suture junction, the nasal and frontal bone fronts overlap extensively, as seen in a schematized sagittal section (Fig. 6A). In addition, undifferentiated mesenchyme lies between the bone fronts, and immature, nonmineralized osteoblasts (called osteoid) are present at the edges of the bones. In sagittal sections obtained at the level of the frontonasal sutures, there are no obvious morphological differences between wild-type and FKO samples before P15 (data not shown). In H&E stained sections at P15, we observe that the frontonasal sutures of wild-type and FKO samples are generally of similar size and shape (Figs. 6B,C). However, upon close examination of the FKO, nasal bone fronts are often thinner in the proximal–distal axis than in matched wild-type sections, which becomes apparent by comparing the distances between (1) the proximal edges of the nasal bone fronts and (2) the nasal bone marrow (Figs. 6B′,C′). To examine this phenomenon in greater detail, nondecalcified snouts were embedded in methyl methacrylate (plastic) and subjected to toluidine blue or Von Kossa staining to visualize bone structure and determine the extent of mineralization in the samples. In wild-type plastic sections at P15, toluidine blue and von Kossa staining illustrate that the nasal bone front is a largely nonossified osteoid projection that forms a posterior extension of the mineralized matrix of the nasal bone proper (Figs. 6D′,F). Matched FKO sections reveal that the overall length of the nasal bone front is similar to that of a wild type, as described above in the paraffin-processed samples. However, the relative contribution of osteoid to this bone front extension in the FKO mutant is much reduced compared to a wild-type sample, and there is a corresponding increase in the mineralized portion (Figs. 6E′,G). These data indicate that the osteoblasts in the mutant nasal bone fronts may prematurely differentiate, which would lead to inappropriate secretion of mineralized matrix and perturbation of postnatal sutural growth.

FKO snouts exhibit nasal bone, nasal suture, and cartilage anomalies

To further investigate the FKO snout anomalies, coronal sections of plastic- and paraffin-embedded samples were examined. At P5, the initial defect observed is an increase in FKO nasal bone thickness (data not shown). As the mutants mature, nasal bone and suture anomalies become more severe and are best illustrated at P15. In the dorsoventral axis, wild-type nasal bones are thick in the midline and become thinner in the lateral regions of the bones, as seen in plastic (Fig. 7A) and paraffin (Figs. 7C,E) sections of P15 samples. The nasal sutures define the midlines of the sections and are aligned with the nasal septum (Figs. 7A,C,E). In contrast, the FKO nasal bones display an increased thickness in the dorsoventral axis within the lateral portion of the bones (Figs. 7B,D), and the nasal sutures are wider in the mediolateral axis (Fig. 7B′), when compared to wild-type samples. In addition, the mutant nasal sutures are slightly off-center and are often laterally angled with respect to the nasal septum (Fig. 7B′,D,F).

Within the nasal cavities, defects in FKO samples are not apparent at P5, are subtle at P10, and more pronounced by P15 (Fig. 7 and data not shown). In P15 wild-type sections obtained 2 mm from the distal tip of the snout, the dorsal portion of the nasal septum contains a triangular patch of cartilage that is intensely stained with toluidine blue, typical of chondrocytes in the proliferative stage of development (Figs. 7A,A′). By 2.5 mm, this septal cartilage has formed a distinct "Y" shape (Fig. 7C). In contrast, the septal cartilage of matched FKO snout sections obtained from the distal halves of the nasal bones contains regions of discontinuity (Figs. 7B,B′,D). Of interest, the unstained regions of the mutant septa contain cells that resemble immature chondrocytes, which may indicate that matrix secretion is impaired in the mutant samples. It is also important to note that the distal tip of the nasal cartilage, which protrudes from the nasal bones, is similar in morphology and composition in wild-type and FKO samples (data not shown). With respect to the superior nasal conchae, the wild-type projections have an "S" shape in

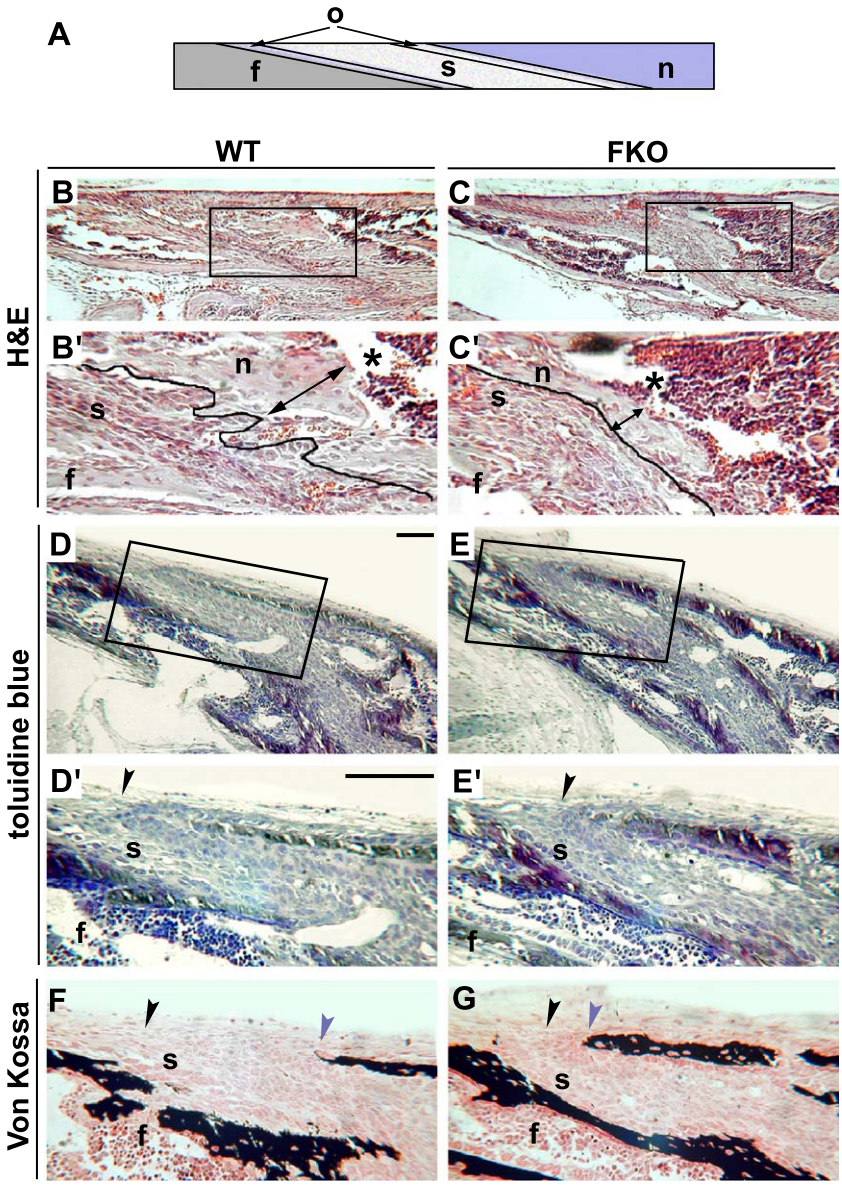

Fig. 6. Examination of the frontonasal sutures of wild-type and FKO snouts at P15. (A) Schematic representation of the frontonasal suture in the sagittal plane. The frontal (f) and nasal (n) bone fronts overlap, and are separated by undifferentiated suture mesenchyme (s). Immature osteoblasts (o) line the bone surfaces at the interfaces with the suture cells. (B–C′) Paraffin sections stained with hematoxylin and eosin (H&E). (B,C) 10× magnification. (B′,C′) 25× (B′) WT and (C′) FKO images, corresponding to boxed regions in B and C, respectively. Note that the (C′) FKO nasal bone front, lined at the proximal surface, is thinner than in the (B′) wild-type sample (double-headed arrows). The nasal bone marrow is indicated with an asterisk (*). (D–G) Plastic sections stained with (D–E′) toluidine blue or (F,G) Von Kossa. (D,E) 10× magnification. (D′–G) 25× (D′,F) WT and (E′,G) FKO images, corresponding to boxed regions in D and E, respectively. Black arrowheads in D′–G mark the proximal limits of the unmineralized nasal bone fronts. Blue arrowheads in E and F mark the proximal limits of the mineralized matrix within the nasal bones. Abbreviations: frontal bone (f), nasal bone (n), suture (s), wild-type (WT). Size bars in D and D′represent 0.1 mm for 10× and 25× panels, respectively.

more distal regions of the snout, while the FKO counterparts are reduced and misshapen (Figs. 7C,D). Interestingly, the septal cartilage and bony projections in more proximal regions of the snout are quite similar to those of wild-type samples (Figs. 7E,F). Together, the data illustrate that the FKO nasal cavity cartilage and bone abnormalities worsen as the mice mature, and are confined to regions underlying the distal halves of the nasal bones.

FKO snouts exhibit reduced FGFR-2 expression levels and proliferation defects

The phenotypes within FKO nasal bones and sutures become apparent between P10 and P21 and appear to be due to a growth defect. Previous studies have shown that late in normal embryogenesis, the edges of the bone fronts within the developing skull express FGFR-2, and are a proliferative cell population, as evidenced by bromodeox-

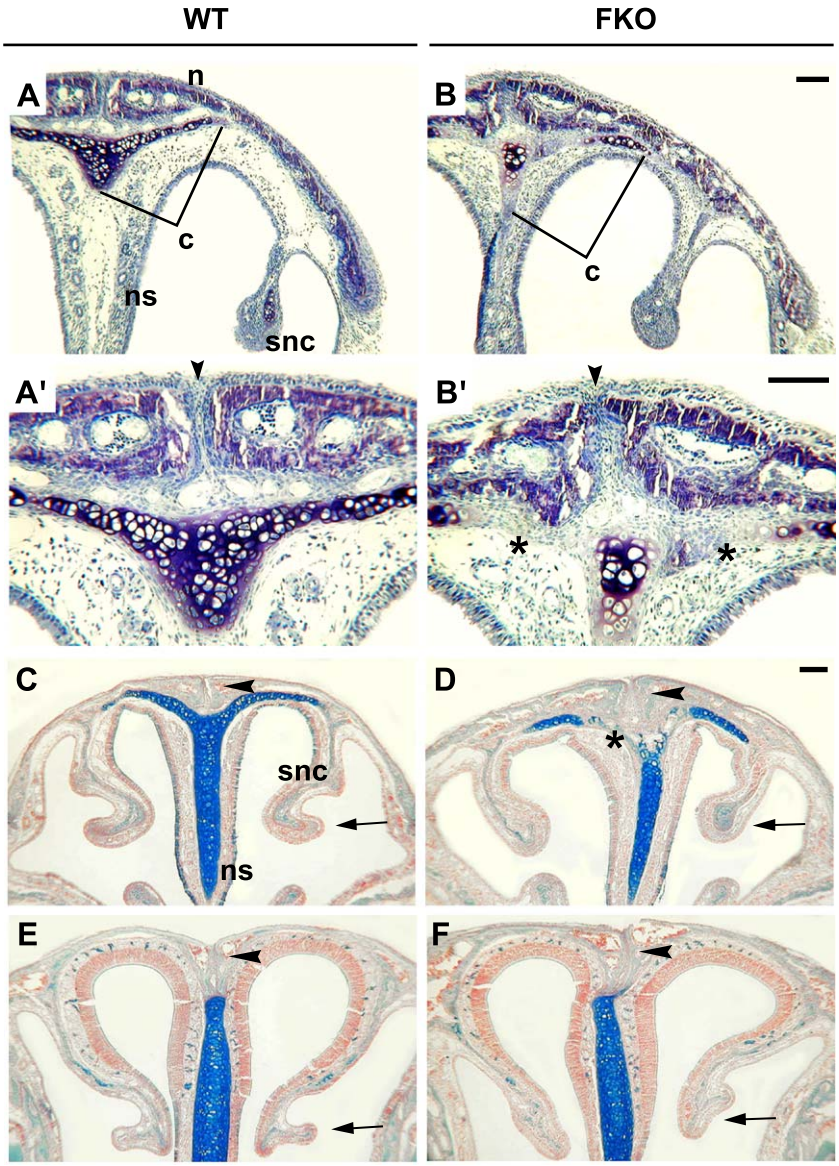

Fig. 7. Coronal section analyses of wild-type and FKO snout samples. (A–B′) Plastic coronal sections stained with toluidine blue. (A,B) 10× plastic sections 2 mm from the distal tip of the snout. (A) Wild-type (WT) and (B) FKO sections are bisected by the nasal septum (ns) and contain projections from the superior nasal conchae (snc). (A) WT nasal bones are thickened at the level of the nasal septum and are tapered laterally; septal cartilage (c) is present ventral to the nasal bones. The (B) FKO nasal bones are more uniform in thickness in the dorsal–ventral axis and the cartilage contains regions of discontinuity in the toluidine blue stain. (A′,B′) 25× plastic sections show disorganization of nasal suture (arrowhead) and the discontinuity of the cartilage is apparent (*) in (B′) FKO samples as compared to (A′) WT. (C–F) Paraffin sections stained with alcian blue, counterstained with nuclear fast red. The (D,F) FKO nasal suture (red arrowhead) is disorganized as compared to (C,E) WT. In the distal snout, (D) FKO septal cartilage contains discontinuous regions (*) and the superior nasal conchae projections are misshapen (red arrow) compared to (C) WT. In more proximal regions of snout, (E) WT and (F) FKO samples have similar septal cartilage structures, and the (F) FKO conchae projections are slightly misshapen. Size bars represent 0.1 mm.

yuridine (BrDU) incorporation (Iseki et al., 1997, 1999). To determine if growth differences exist between wild-type and FKO frontal and nasal bones before the manifestation of the mutant anomalies, we performed FGFR-2 ISH and BrDU assays. Ten pairs of skulls were processed for whole-mount FGFR-2 ISH. At E17.5, the bone fronts of both wild-type and FKO parietal and interparietal bones have similar levels of FGFR-2 expression (data not shown). With respect to the frontal bones, wild-type samples exhibit diffuse expression along the medial surfaces, and have slightly stronger expression in the bone fronts adjacent to the facial sutures (data not shown). In the nasal regions, nasal bones exhibit strong perimeter expression, and the entire surfaces of the premaxillary bones express FGFR-2 (Fig. 8A). Mutant littermates exhibit a range of FGFR-2 expression patterns in the developing facial complex. Approximately 50% of the FKO nasal bones have perimeter staining patterns similar to wild-type littermates, but the levels are slightly reduced (data not shown). Other mutants exhibit obvious reductions

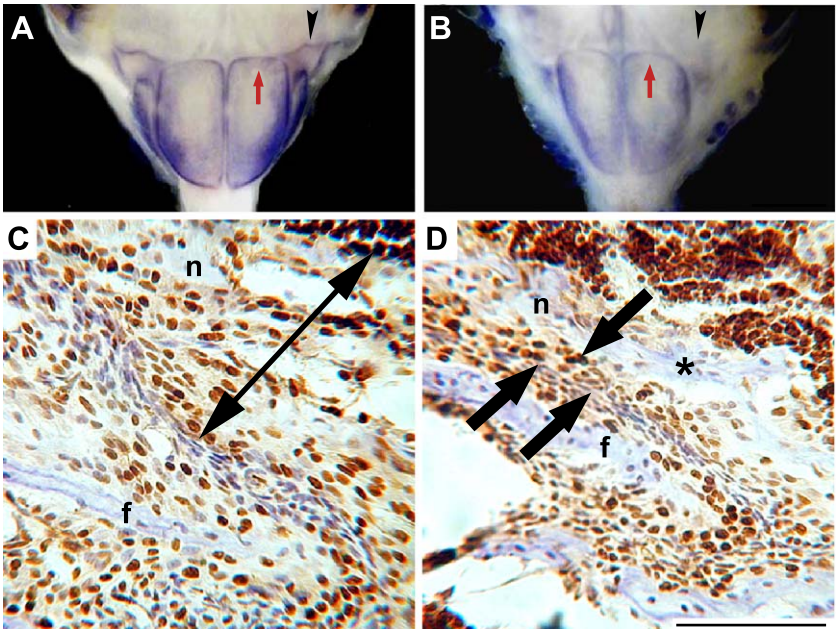

Fig. 8. FGFR-2 and PCNA expression studies. (A,B) Whole-mount FGFR-2 ISH at E17.5. (A) Wild-type (WT) nasal (red arrows) and frontal (arrowheads) bone fronts show strong FGFR-2 expression. (B) In contrast, the FKO snout exhibits reduced expression in both nasal and frontal bone fronts. (C,D) PCNA expression at P15. (C) WT samples contain PCNA-positive (brown) nuclei throughout the nasal bone front adjacent to the frontonasal suture (double-headed arrow). (F) FKO frontonasal sutures contain positive cells within the interface between the suture mesenchyme and the nasal bone fronts (arrows). The nasal bone fronts (*) of mutant samples are largely PCNA-negative. Abbreviations: nasal bone (n) and frontal bone (f). Size bar in B represents 1.0 mm. Size bar in D represents 0.1 mm.

in FGFR-2 expression levels in the most proximal and distal regions of the nasal bones (Fig. 8B), as well as a decrease in the suture-associated expression in the frontal bones. In addition, mutants with more obvious reductions in nasal bone expression often have less premaxillary bone staining (Fig. 8B).

BrDU studies were subsequently carried out at P1, and cell counts were obtained from the nasal and frontonasal sutures as well as within the nasal septum. Growth rates were similar between wild-type and FKO samples in both the nasal and frontonasal sutures. In contrast, in the nasal septum approximately 5% of the cells were proliferating in wild-type samples, while approximately 2.7% were proliferating in the matched FKO sections ($n = 3$, $P < 0.005$). This finding may partially explain the septal cartilage defects we observe in the FKO snouts. We next examined BrDU incorporation in the frontonasal sutures in P5 and P15 sagittal sections, but there were no significant differences between wild-type and mutant samples at either stage (data not shown). At P15, the BrDU labeling index was less than 1% for both wild-type and mutant samples. Therefore, we examined the expression of the proliferation marker PCNA at this stage. In the frontonasal sutures, wild-type and FKO samples exhibit PCNA expression within the suture mesenchyme adjacent to both the nasal and frontal bones (Figs. 8C,D). In most sections examined from wild-type samples, most of the cells within the nasal bone fronts are also positive for PCNA (Fig. 8C). In contrast, sections from the nasal bone fronts of the FKO samples tend to contain a ridge of PCNA-positive cells adjacent to the suture cells, while the remaining cells of the bone front are negative (Fig. 8D). Of interest, apoptosis was also investigated at P1, P5, and P15, and no aberrant cell death occurs in the FKO samples at these stages (data not shown). Taken together, these data suggest that slight reductions in early growth factor signaling and perturbed postnatal cell proliferation are involved in the defects observed in the FKO snouts, rather than inappropriate cell death.

Loss of AP-2α from the FNP results in vascular defects

In addition to the overt bone anomalies identified in FKO skull preparations, we observed vascular reductions within the mutant nasal bones as early as P15 (data not shown). At P30, wild-type nasal bones have a characteristic vascular pattern that extends from the frontonasal suture to the middle portion of the bones. In addition, a thin line of vessels extends toward the distal edges of each of the nasal bones at the facial midline (Fig. 9A′). In contrast, FKO samples often have a less regular vascular network adjacent to the frontonasal sutures, which does not reach the middle region of the nasal bones, and the midline extensions are small or absent (Fig. 9B′ and data not shown). In the FKO snout pictured in Fig. 9B, blood vessels are visible in the distal regions of the nasal bones, but two other mutant samples analyzed were devoid of vasculature in this region (data not shown). Importantly, wild-type and FKO frontal bones have similar vascular patterns (Figs. 9A,B), indicating

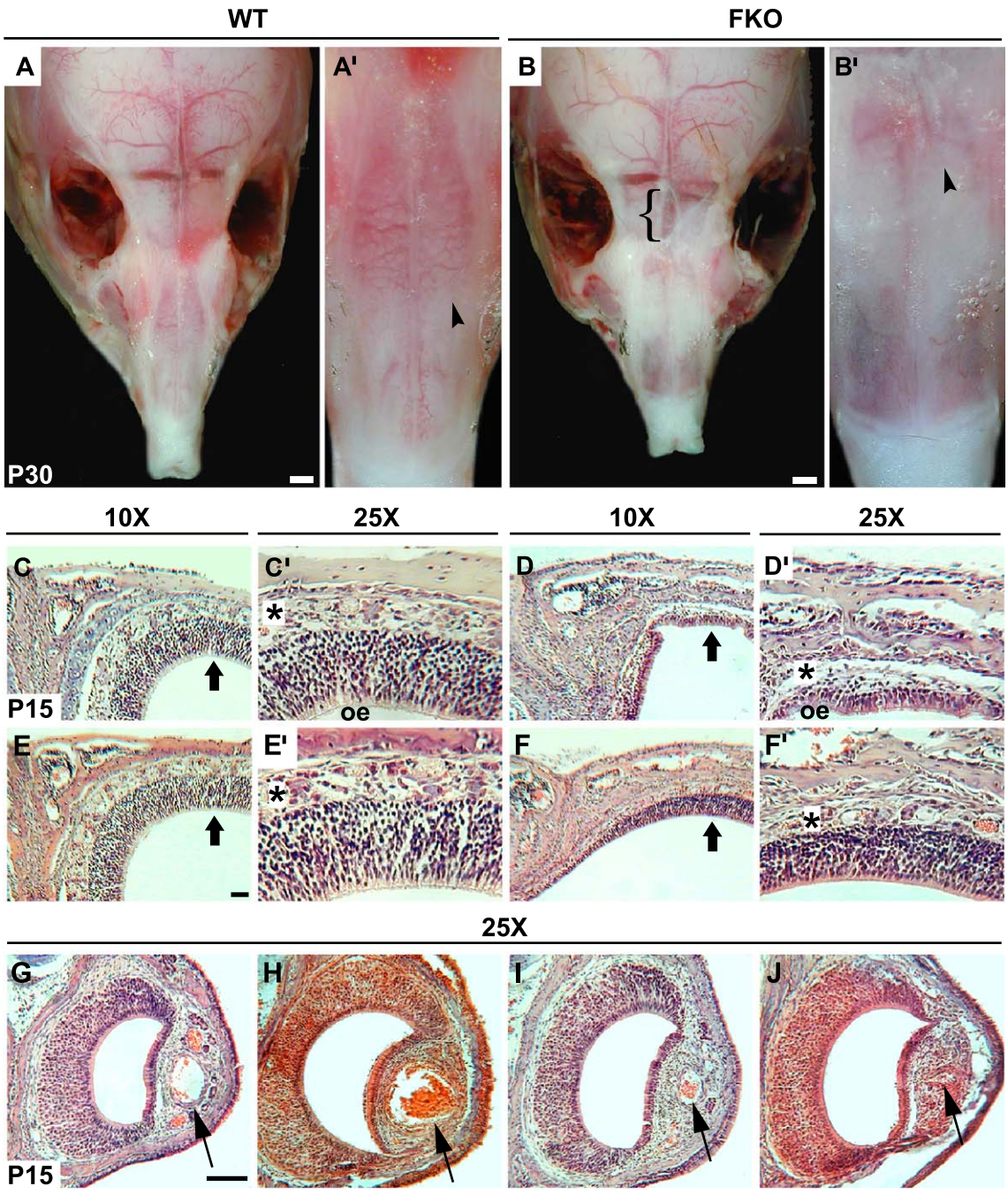

Fig. 9. Vascular anomalies in FKO pups. (A,B) Nasal bone vascular patterns in whole-mount preparations at P30. (A) Wild-type (WT) skull. (A′) WT nasal bones. Note that the blood vessel network within the proximal two-thirds, and the thin extensions in the midline of the distal third of the snout. (B) FKO skull. (B′) FKO nasal bones. The vascular network is reduced and disorganized compared to (A′). Arrowheads mark the distal limits of the nasal bone vascular networks associated with the frontonasal sutures. The bracket in B delimits the interfrontal bone. (C–J) Paraffin sections stained with H&E to visualize nasal cavity structures at P15. Note: C, D are distal to, and E, F are proximal to the frontonasal sutures. (C–F) are 10×, (C′–F′, G–J) are 25×, and C′–F′correspond to the regions indicated with arrows in C–F. At P15, the (D,F) FKO mucosa (*) and olfactory epithelia (oe) are thinner than in (C,E) WT samples. The VNO vessels (thin arrows) are also reduced in (I,J) FKO samples, as compared to (G,H) WT littermates. Size bars in A and B represent 1.0 mm. Size bars in E and G represent 0.1 mm for 10× and 25× panels, respectively.

that the major vessel anomalies are confined to the snout in the mutant samples.

In paraffin sections, differences are not apparent between wild-type and mutant samples from E13.5 through P5 (data not shown). However, we found that among the eight pairs of wild-type and mutant snouts sectioned between P10 and P15, approximately 50% of the FKO samples exhibit a noticeably reduced thickness of the mucosa that specifically underlies the nasal bones (Figs. 9C–F′and data not shown). Discerning individual veins and arteries within the mucosal mesenchyme

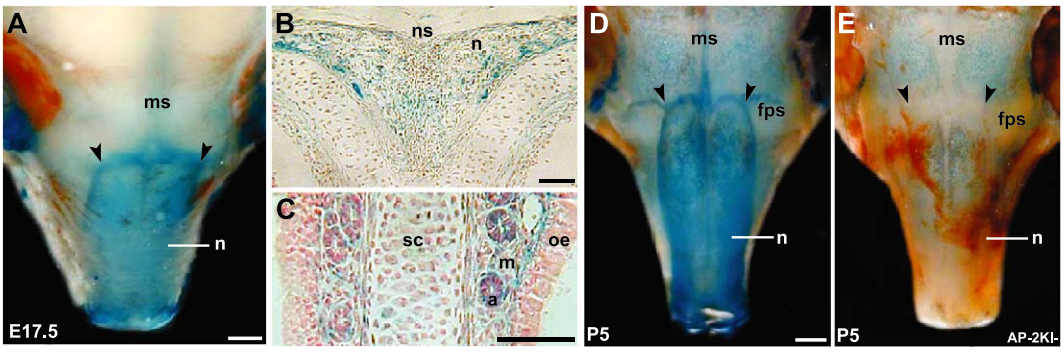

Fig. 10. AP-2α is expressed in late embryonic and postnatal skull tissues. (A) AP-2KI-associated β-galactosidase activity is present in the nasal bone (n), frontonasal suture (arrowheads), and metopic suture (ms) at E17.5. (B,C) In sections, additional expression is visible in (B) the nasal suture (ns). (C) In the region of the nasal septum, the septal cartilage (sc), mucosal mesenchyme (m), and arteries (a) are positive. (D) At P5, expression persists in the nasal bones, the frontonasal and metopic sutures, and expression is strong in the frontal–premaxillary sutures (fps). (E) AP-2KI-negative P5 sample illustrates background staining in frontal, nasal, and premaxillary bones. Size bars represent 1.0 mm.

is difficult, but there appear to be fewer vessels within the thinner regions of the mutant mucosa, accompanied by reductions in the thickness of the adjacent olfactory epithelia (Figs. 9D′,F′). In addition, we found that the large vessels associated with the vomeronasal organ (VNO) are reduced in all FKO mice when compared to wild-type littermates (Fig. 9, compare littermates G,I and H,J).

VEGF and VEGFR-2 are essential for vascular development, and studies have demonstrated that they are transcriptional targets of AP-2α (Gille et al., 1997; Papetti and Herman, 2002; Ronicke et al., 1996). Therefore, we performed immunohistochemistry for VEGF and VEGFR-2 in wild-type and mutant samples at several stages between E15.5 and P15, but observed no apparent differences between the expression of these molecules at any of the stages examined (data not shown). From these results AP-2α is clearly not affecting the vasculature by a direct affect on VEGF and VEGFR-2 expression levels, although we cannot exclude the possibility that post-translational changes in VEGF activation may still occur during pathology (Colnot et al., 2003).

Postnatal AP-2α expression in the craniofacial complex correlates with AP-2CRE activity

Analyses of the FKO phenotypes suggested two basic possibilities with respect to the roles of AP-2α in facial development. First, loss of AP-2α from the embryonic FNP, a tissue in which the gene is expressed, may be sufficient to hinder proper postnatal growth. Second, if AP-2α is expressed in postnatal facial structures, loss of the gene from the derivatives affected by AP-2CRE might be detrimental to snout outgrowth. Therefore, we have characterized AP-2α expression at late embryonic and early postnatal stages in the craniofacial complex using the AP-2KI line of

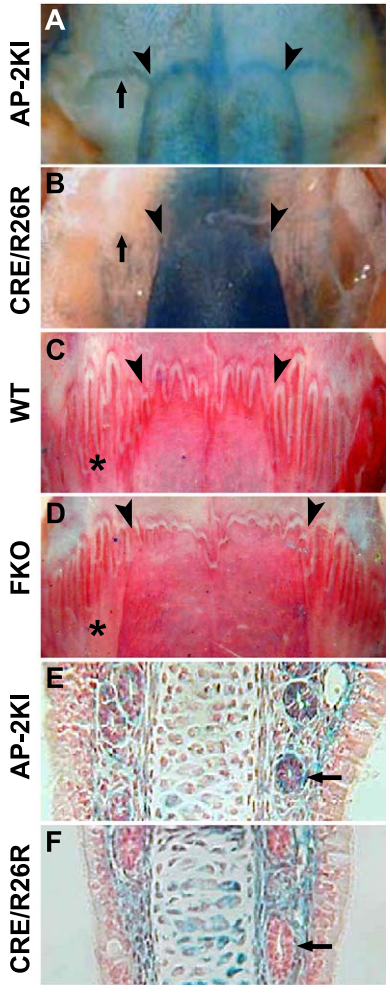

Fig. 11. Correlation of AP-2α expression and AP-2CRE/R26R β-galactosidase activities. Alignments of whole-mount skull preparations to compare (A) AP-2KI- and (B) AP-2CRE-dependent β-galactosidase activities with (C) WT and (D) FKO suture interdigitation patterns. (A–D) Arrowheads indicate the frontonasal sutures, which are positive for (A) AP-2α and (B) AP-2CRE. (A,B) Arrows indicate the frontal–premaxillary sutures, which express AP-2α, but do not contain AP-2CRE activity. (C,D) Asterisks (*) mark the frontal–premaxillary suture interdigitation patterns. In sections, (E) AP-2α and (F) AP-2CRE are present in the septum and mucosa. The blood vessels (red arrows) within the mucosa express (E) AP-2α but do not possess (F) AP-2CRE activity.

mice (Brewer et al., 2002). In this line, the *lacZ* gene was introduced into the AP-2α locus, and β-galactosidase activity recapitulates endogenous AP-2α expression in heterozygous animals. AP-2α expression is described below for skull preparations from various stages, and compared to the aforementioned AP-2CRE/R26R β-galactosidase activities (Fig. 2). Importantly, the structures in common are tissues that lack functional AP-2α in FKO mutant mice.

In whole-mount preparations at E15.5 and E17.5, AP-2KI-associated β-galactosidase activity is detected in the nasal regions of the embryos and is weak in the anterior portion of the metopic sutures (Fig. 10A and data not shown). In serial sections at E15.5 and E17.5, AP-2α is expressed in the nasal bones and sutures as well as in the mucosal mesenchyme and associated blood vessels (Figs. 10B,C and data not shown). In addition, nasal septal cartilage and the primordia of the superior nasal conchae exhibit weak expression at E15.5 that is less intense by E17.5 (data not shown).

At P1 and P5, AP-2α expression persists in nasal region tissues, and becomes stronger in the metopic suture (Fig. 10D and data not shown). In addition, β-galactosidase activity is present in all suture junctions between the frontal bones and the nasal, premaxillary, and maxillary bones. There is also activity in the sutures separating the nasal and premaxillary bones. Expression in the facial sutures is maintained in P10 skulls and continues through P15 (data not shown).

With respect to the tissues in which AP-2α may be required, AP-2α expression and AP-2CRE/R26R β-galactosidase activities coincide in the nasal bones, the frontonasal, nasal, and metopic sutures (Figs. 11A,B), the nasal cavity cartilage and conchae projections, and the mesenchyme of the vascular mucosa (Figs. 11E,F). Thus, we would predict that the defects in the FKO mouse result from the deletion of AP-2α in one or more of the above tissues. Note that AP-2α is additionally expressed in the vessels of the mucosa and within the frontal–premaxillary suture, structures that do not possess AP-2CRE-mediated β-galactosidase activity (Figs. 11A,B,E,F). Therefore, these tissues are unlikely to be primary sites of the defects observed in FKO snouts.

Discussion

Conditional mutagenesis is a powerful approach to address the roles of genes in specific tissues. The AP-2CRE allele described in this study is an important tool for understanding how a particular gene functions in a subset of cranial neural crest and head mesenchyme tissues, as well as within the distal limb structures. Use of this CRE allele to eliminate AP-2α from the FNP generated a new mouse model of midfacial hypoplasia, in which a unique subset of craniofacial tissues is affected. In the FKO mice, we hypothesize that the loss of AP-2α from these FNP derivatives results in two "primary" defects that are responsible for the mutant phenotypes. First, premature mineralization of the FKO nasal bone fronts inhibits growth at the frontonasal suture junctions, ultimately truncating the mutant facial complex. Second, the reductions in the FKO nasal region vasculature likely account for the cartilage and bone defects identified in the mutant nasal cavities.

Targeting CRE recombinase to the developing FNP and limbs

To direct the expression of CRE recombinase to the developing mouse FNP, we utilized a previously characterized human AP-2α FNP and limb mesenchyme enhancer element (Zhang and Williams, 2003). AP-2CRE activity begins between E8.75 and E9.0 in the lateral regions of the head and migrating cranial neural crest, and it is robust in the FNP proper from E9.5 onward. In the limbs, AP-2CRE-mediated β-galactosidase activity is first detected around E9.5, and is maintained in the distal two-thirds of the limb bud and subsequent muscular and skeletal elements.

Derivatives of the embryonic FNP marked in AP-2CRE/R26R skulls include the nasal bones, the facial and metopic sutures, as well as the nasal cavity cartilage and mucosal mesenchyme. It is interesting to note that β-galactosidase activity is also observed in the frontal bones and the premaxilla, in regions immediately adjacent to AP-2CRE-positive sutures. Thus, the enzyme activities likely reflect the nature of suture cell recruitment to the bone fronts for membrane bone growth to occur. Importantly, the structures marked by AP-2CRE are a specific subset of the cranial neural crest derivatives identified in embryos and pups containing *Wnt1-Cre* and R26R, in which the frontal bones, the coronal sutures, and part of the sagittal sutures are also positive (Jiang et al., 2002). Therefore, the AP-2CRE line is a unique tool that will be extremely useful for loss of function studies within craniofacial neural crest-derived structures.

FKO snout truncation is due to impaired growth at the frontonasal suture

Tissue-specific deletion of AP-2α was accomplished using the AP-2CRE and Alflox conditional alleles, and the resulting FKO embryos lack AP-2α expression in FNP and limb bud mesenchyme. Unexpectedly, given the severe craniofacial defects observed in previous AP-2α mutant studies (Nottoli et al., 1998; Schorle et al., 1996; Zhang et al., 1996), FKO embryos do not have obvious facial anomalies. Rather, FKO pups display postnatal craniofacial shortening and interorbital hypertelorism that are subtle at P15, but become more obvious as the mice mature. Interestingly, the FKO mice do not exhibit forelimb defects, which illustrates that loss of AP-2α after E9.5 in the distal mesenchyme is not sufficient to affect patterning in the zeugopod. This latter observation indicates that AP-2α may be required earlier in limb development, or perhaps within a different tissue, such as the limb ectoderm.

Elongation of the postnatal craniofacial complex in wild-type mice is characterized by the outgrowth of the nasal and premaxillary bones, coupled with an increasing complexity of the interdigitation patterns within the frontonasal and frontal-premaxillary sutures. In the FKO snouts, both the nasal and frontal bones are truncated in their proximodistal axes, and the nasal bones are visibly shorter than the adjacent premaxillary bones. Several lines of evidence support the conclusion that the lack of nasal and frontal bone outgrowth in the mutants is primarily due to impaired growth at the frontonasal suture caused by the absence of AP-2α within this junction. First, the frontonasal sutures are major sites of postnatal AP-2α expression, and the cells that generate these structures are efficiently targeted by AP-2CRE during embryogenesis (Figs. 11A,B). Second, in contrast to wild-type samples, the FKO frontonasal sutures do not become extensively interdigitated, and they exhibit a posterior displacement with respect to the frontal-premaxillary sutures (Figs. 11C,D). With respect to the cause of the FKO frontonasal suture growth defects, sagittal sections illustrate that the mutant nasal bone fronts are very similar to those of wild-type samples through P10, but by P15 they contain fewer undifferentiated, nonmineralized osteoblasts. These characteristics are potentially caused by the premature differentiation and subsequent mineralization of osteoblasts within the proximal region of the FKO nasal bone fronts, both of which are hallmarks of craniosynostosis disorders (Fragale et al., 1999; Zhang et al., 2002). In contrast, mineralization levels are comparable between wild-type and FKO distal nasal bone sections, which indicates that the mineralization defects in the mutants are specific to the nasal bone fronts. It is important to note that additional features of the FKO snouts can be attributed to a lack of frontonasal suture growth. Without growth at suture junctions, skull bones can increase in thickness but not in length (Mao, 2002). In addition, studies have shown that physically restraining the frontonasal suture results in nasal bone truncation as well as shortening of the ethmoid structures that underlie the nasal bones (Babler et al., 1987; Persing et al., 1991). Taken together, these data indicate that growth inhibition at the frontonasal suture could cause the increased thickness of the mutant nasal bones, as well as the truncation of the entire craniofacial complex observed in FKO snouts.

In both human and mouse, suture function has been linked to the appropriate expression and activity of FGFR-2, and many human craniosynostosis cases have been associated with mutations in FGFR-2 that lead to aberrant receptor activation (Reardon et al., 1994; Wilkie et al., 1995; for reviews see Opperman, 2000; Ornitz and Marie, 2002; Wilkie and Morriss-Kay, 2001). FGFR-2 is expressed in the osteogenic fronts of the membrane bones within the developing skull, and its expression coincides with bone front proliferation in E17.5 mouse embryos (Iseki et al., 1997, 1999). A recent study in the mouse has recapitulated human coronal suture synostosis by altering FGFR-2 expression, through the elimination of the FGFR-2-IIIC isoform from the embryonic skeletogenic mesenchyme (Eswarakumar et al., 2002). This defect is due to a loss of proliferating cells in the frontal and parietal bone fronts, which leads to reduced osteogenic potential and premature differentiation (Eswarakumar et al., 2002). Given the connection between FGFR-2 and synostosis, we examined FGFR-2 expression in the relevant sutures of FKO and wild-type skulls. In contrast to normal littermates, we detect slightly weaker and variable FGFR-2 expression in the mutants, but at early postnatal time points this did not coincide with any significant difference in suture cell proliferation. However, with PCNA staining at P15, we were able to detect differences between wild-type and FKO samples. In wild-type frontonasal sutures, the nasal bone fronts are largely PCNA-positive, which likely reflects the undifferentiated state of the cells. In contrast, the FKO nasal bone fronts are mostly PCNA-negative, correlating with the more differentiated nature of the mutant bone front. Therefore, we postulate that in FKO embryos, there is a defect in the establishment of critical bone fronts that ultimately reduces the postnatal growth potential of the nasal bones. Differential growth activity along the length of the frontonasal suture may also explain the craniofacial defects seen in a low percentage of heterozygous AP-2α-null mice (Nottoli et al., 1998). In affected heterozygotes, we see a curvature of the snout that results in misalignment of the upper and lower incisors. In this instance, we hypothesize that the reduced levels of AP-2α in the facial complex reach a threshold at which the bone fronts may not function effectively. If only one side of the frontonasal suture was adversely affected, then the adjacent frontal and nasal bones would be shorter, causing the snout to curve towards the affected side.

In addition to defects within the frontonasal sutures, the metopic sutures of FKO mice display ectopic interfrontal (IF) bone. Because a substantial percentage of wild-type samples also contain IF bone, and only mice with the FKO genetic combination display snout truncations, there is not an absolute causal relationship between the presence of the ectopic bone and frontonasal suture defects. One potential cause of the ectopic bone is the mixture of genetic backgrounds that occurs in our breeding scheme. Strain mixing has been associated with increasing the propensity of IF bone in wild-type specimens (Fukuta et al., 1988), and each allele required in our study was maintained within a different strain of mouse. However, because of the 100% penetrance of the IF bone in FKO samples, it is also possible that the loss of AP-2α directly affects the metopic suture mesenchyme by promoting osteogenesis. Such a conclusion is supported by the observations that the mutant nasal bone fronts also appear to be affected by inappropriate osteogenic differentiation.

Finally, an intriguing field of suture biology is dedicated to understanding how biomechanical forces contribute to suture growth and interdigitation, and the subsequent lon-

gitudinal growth of skull and facial bones (reviewed in Mao, 2002). For example, mice fed a granulated diet exhibit reduced nasal bone lengths when compared to mice fed on a solid diet, indicating that increased masticatory function promotes growth of the nasal bones (Kiliaridis et al., 1985; Tokimasa et al., 2000). Studies have also shown that application of exogenous oscillatory mechanical strain stimulates osteogenic proliferation within the frontonasal sutures (Mao et al., 2003). Together, the data show that suture junctions are capable of responding to mechanical stimuli by proliferating and differentiating, which subsequently facilitates the elongation of adjacent bones. Because growth is perturbed at the FKO frontonasal suture junctions, it is interesting to consider that AP-2α might play a role in the signaling pathways that communicate sutural mechanical strain.

Vascular deficiency contributes to FKO nasal cavity anomalies

Vascular defects were observed in FKO nasal bones, the mucosa lining the nasal cavity, and the VNO. All mutants processed between P10 and P15 display obvious reductions in the sizes of the VNO vessels, and we speculate that some degree of vascular dysfunction is present in all FKO pups. Importantly, AP-2α is expressed throughout the mucosa and blood vessels, while AP-2CRE activity is confined to the mesenchyme surrounding the vessels (Figs. 11E,F). This suggests that the vascular reductions in FKO snouts are due to defects within the mucosal environment in which the blood vessels develop.

We hypothesize that the abnormalities within the FKO superior nasal conchae, septal cartilage, and olfactory epithelium are secondary to the reduction in snout vasculature as vascular defects are known to disrupt growth of bone and cartilage (Gerber et al., 1999; Maes et al., 2002; Zelzer et al., 2002, reviewed in Gerber and Ferrara, 2000). With respect to the conchae, which ossify endochondrally, the lack of growth may be attributed to defects in vascular invasion that occur in the postnatal period. In contrast to membranous and endochondral bones, cartilage is an avascular tissue that relies on diffusion from adjacent blood vessels for obtaining oxygen and subsequently removing waste (Zelzer et al., 2002, reviewed in Blair et al., 2002). Therefore, the mucosal vascular network likely supplies the necessary oxygen required for the postnatal growth and maintenance of the adjacent nasal septal cartilage. We speculate that in the FKO mucosa, the reduced numbers of vessels negatively affect the nearby cartilage by impairing matrix secretion. It has been shown in vitro that hypoxic conditions suppress the expression of the α subunit of Type II collagen, a major component of the cartilage matrix (Grimshaw and Mason, 2001). Of interest, the intense toluidine blue stain observed in both wild-type and FKO septal cartilage correlates with high levels of Type II collagen expression, and is typical of proliferative chondrocytes (Naumann et al., 2002). In the FKO samples, the regions that lack intense cartilage stain do contain cells that resemble immature chondrocytes, and they are in regions associated with reduced numbers of vessels. Thus, in the FKO nasal cavity, hypoxic conditions may exist in FKO snouts, which would suppress Type II collagen expression in adjacent chondrocytes and lead to patches of cells that are devoid of toluidine blue stain. Similar to the septal cartilage, the olfactory epithelium is adjacent to and likely relies upon the vascular mucosa for proper nourishment and subsequent development. The defects within the epithelial layers are truly secondary, as AP-2α and AP-2CRE are not present in these tissues. The reductions in the FKO olfactory epithelia also raise the intriguing possibility that odor detection is impaired in the mutant mice. Therefore, the FKO mouse mutant may be an interesting model in which to study the influences of the vascular system upon the postnatal development and function of the olfactory system.

We cannot exclude the possibility that AP-2α may directly regulate cartilage formation, as AP-2α expression and AP-2CRE activity do coincide in the nasal septum and superior conchae primordia in embryogenesis (see Figs. 11E,F). Therefore, AP-2α is lost from the cartilaginous precursors of these structures in FKO snouts. However, we do not favor this direct regulatory hypothesis for several reasons. First, the expression of AP-2α in the cartilage and the onset of the defects are inversely correlated. AP-2α expression in these elements is greatest during embryogenesis and then becomes less robust as the mice mature. In contrast, wild-type and FKO nasal conchae and septal cartilage structures are indistinguishable through P5, the defects in these structures appear around P10, and then subsequently worsen as the mice mature. Second, the cartilage defects are confined within the distal portions of the nasal bones, regions in which the vasculature is most noticeably reduced in FKO samples. Thus, these observations further support the notion that the hypoplasia of the nasal septum and conchae result from reduced vascular functions.

At this juncture, the possibility remains that reduced vascular functions within the FKO snout contribute to the frontonasal suture and/or nasal bone elongation defects. However, our current hypothesis is that the vascular reductions in FKO snouts do not impair growth of the frontonasal suture. Rather, it is the loss of AP-2α from the nasal bone fronts and associated suture tissues that results in aberrant mineralization and growth inhibition of the frontonasal junction. This conclusion is based on the observations that AP-2α is robustly expressed in the nasal bones and associated suture mesenchyme, and that the snout vasculature within regions immediately adjacent to the frontonasal sutures are similar in wild-type and FKO samples. In contrast, the blood vessels within the distal halves of the nasal bones are most compromised in the mutants. In this study, we cannot yet distinguish whether

abnormal vascular development impairs the distal growth of the nasal bone, or if nasal bone defects perturb vessel growth. Experiments with additional CRE recombinase lines specific for either bone or vasculature will be needed to resolve these issues. Nevertheless, the vessel reductions in the distal snout likely exacerbate the FKO nasal bone truncation by reducing outgrowth potential. Finally, whether the lack of vasculature in the nasal cavity mucosa is a direct result of the loss of AP-2α from the mucosal mesenchyme, or results indirectly from defects in the overlying nasal bones, the alteration in blood supply would cause the defects found in septal cartilage and superior nasal conchae projections.

In conclusion, the FKO mutants represent a new mouse model of midfacial hypoplasia. Ultimately, determining how craniofacial outgrowth is compromised in the FKO snouts at the cellular and molecular levels will increase our comprehension of how facial tissues maintain growth sites in the postnatal facial skeleton. Because a variety of tissues are affected in these mutants, it will be interesting to eliminate AP-2α from even more discrete tissue or cell subtypes to determine where loss of the gene is most detrimental to craniofacial development as more CRE lines become available. Identification of the specific cellular processes affected in the tissues that require AP-2α will lead to a better understanding of how this critical transcription factor functions in mammalian development.

Acknowledgments

We thank Nancy Trioano, Christiane Coady, and Mark Horowitz of the Yale University Core Center for Musculoskeletal Disorders for the plastic tissue processing, sectioning, and staining, and general guidance with the handling of postnatal bone samples. Microinjection of the AP-2CRE transgene was performed by Carole Arthur at the Yale University and Yale Cancer Center Animal Genomics Services. We thank Jian Huang and Stephanie Donaldson for the generation and expansion of the Alflox line of mice for use with the AP-2CRE strain, as well as Dana Peck and Monica Vella for assistance with characterizing the AP-2CRE mouse line. We thank Gail Martin (NLS-CRE plasmid), Philippe Soriano (R26R mice), Janet Rossant (FGFR-2 probe) for their generous gifts. We thank Stephanie Brewer for useful discussions throughout this study, and for critically reading this manuscript. We also thank Mark Lewandoski, Charles Greer, Helen Treloar, Riccardo Chiusaroli, Thomas Carpenter, Linda Sandell, and Jimmy Huang for helpful discussion, as well as Hsin Juan and Lori Sussel for comments on the manuscript. We are also grateful to Professor Frank Ruddle and the members of the Williams and Ruddle laboratories for their assistance. This work was supported by NIH R01 DE12728 (T.W.).

References

Adab, K., Sayne, J.R., Carlson, D.S., Opperman, L.A., 2002. Tgf-beta1, Tgf-beta2, Tgf-beta3 and Msx2 expression is elevated during frontonasal suture morphogenesis and during active postnatal facial growth. Orthod. Craniofac. Res. 5, 227–237.

Babler, W.J., Persing, J.A., Nagorsky, M.J., Jane, J.A., 1987. Restricted growth at the frontonasal suture: alterations in craniofacial growth in rabbits. Am. J. Anat. 178, 90–98.

Blair, H.C., Zaidi, M., Schlesinger, P.H., 2002. Mechanisms balancing skeletal matrix synthesis and degradation. Biochem. J. 364, 329–341.

Brewer, S., Jiang, X., Donaldson, S., Williams, T., Sucov, H.M., 2002. Requirement for AP-2α in cardiac outflow tract morphogenesis. Mech. Dev. 110, 139–149.

Brewer, S., Feng, W., Huang, J., Sullivan, S., Williams, T. Wnt1-Cre mediated deletion of AP-2α causes multiple neural crest related defects. Dev. Biol., in press.

Ciruna, B.G., Rossant, J., 1999. Expression of the T-box gene eomesodermin during early mouse development. Mech. Dev. 81, 199–203.

Cohen, M.F., 2000. Suture Biology. Oxford Univ. Press, New York.

Colnot, C., Thompson, Z., Miclau, T., Werb, Z., Helms, J.A., 2003. Altered fracture repair in the absence of MMP9. Development 130, 4123–4133.

Couly, G.F., Coltey, P.M., Le Douarin, N.M., 1992. The developmental fate of the cephalic mesoderm in quail-chick chimeras. Development 114, 1–15.

Couly, G.F., Coltey, P.M., Le Douarin, N.M., 1993. The triple origin of skull in higher vertebrates: a study in quail-chick chimeras. Development 117, 409–429.

el Ghouzzi, V., Le Merrer, M., Perrin-Schmitt, F., Lajeunie, E., Benit, P., Renier, D., Bourgeois, P., Bolcato-Bellemin, A.L., Munnich, A., Bonaventure, J., 1997. Mutations of the TWIST gene in the Saethre–Chotzen syndrome. Nat. Genet. 15, 42–46.

Eswarakumar, V.P., Monsonego-Ornan, E., Pines, M., Antonopoulou, I., Morriss-Kay, G.M., Lonai, P., 2002. The IIIc alternative of Fgfr2 is a positive regulator of bone formation. Development 129, 3783–3793.

Fragale, A., Tartaglia, M., Bernardini, S., Di Stasi, A.M., Di Rocco, C., Velardi, F., Teti, A., Battaglia, P.A., Migliaccio, S., 1999. Decreased proliferation and altered differentiation in osteoblasts from genetically and clinically distinct craniosynostotic disorders. Am. J. Pathol. 154, 1465–1477.

Fukuta, K., Goto, N., Inoue, T., Imamura, K., Mikami, H., Onishi, A., 1988. Appearance of interfrontal bone in chimeric mouse. Jikken Dobutsu 37, 165–170.

Gerber, H.P., Ferrara, N., 2000. Angiogenesis and bone growth. Trends Cardiovasc. Med. 10, 223–228.

Gerber, H.P., Hillan, K.J., Ryan, A.M., Kowalski, J., Keller, G.A., Rangell, L., Wright, B.D., Radtke, F., Aguet, M., Ferrara, N., 1999. VEGF is required for growth and survival in neonatal mice. Development 126, 1149–1159.

Gille, J., Swerlick, R.A., Caughman, S.W., 1997. Transforming growth factor-alpha-induced transcriptional activation of the vascular permeability factor (VPF/VEGF) gene requires AP-2-dependent DNA binding and transactivation. EMBO J. 16, 750–759.

Grimshaw, M.J., Mason, R.M., 2001. Modulation of bovine articular chondrocyte gene expression in vitro by oxygen tension. Osteoarthr. Cartil. 9, 357–364.

Hogan, B., Beddington, R., Constantini, F., Lacy, E., 1994. Manipulating the Mouse Embryo. Cold Spring Harbor Laboratory Press, Cold Spring Harbor, NY.

Howard, T.D., Paznekas, W.A., Green, E.D., Chiang, L.C., Ma, N., Ortiz de Luna, R.I., Garcia Delgado, C., Gonzalez-Ramos, M., Kline, A.D., Jabs, E.W., 1997. Mutations in TWIST, a basic helix-loop-helix transcription factor, in Saethre–Chotzen syndrome. Nat. Genet. 15, 36–41.

Iseki, S., Wilkie, A.O., Heath, J.K., Ishimaru, T., Eto, K., Morriss-Kay,

G.M., 1997. Fgfr2 and osteopontin domains in the developing skull vault are mutually exclusive and can be altered by locally applied FGF2. Development 124, 3375–3384.

Iseki, S., Wilkie, A.O., Morriss-Kay, G.M., 1999. Fgfr1 and Fgfr2 have distinct differentiation- and proliferation-related roles in the developing mouse skull vault. Development 126, 5611–5620.

Jabs, E.W., Muller, U., Li, X., Ma, L., Luo, W., Hayworth, I.S., Klisak, I., Sparks, R., Warman, M.L., Mulliken, J.B., Snead, M.L., Maxson, R., 1993. A mutation in the homeodomain of the human MSX2 gene in a family with autosomal dominant craniosynostosis. Cell 75, 443–450.

Jiang, X., Iseki, S., Maxson, R.E., Sucov, H.M., Morriss-Kay, G.M., 2002. Tissue origins and interactions in the mammalian skull vault. Dev. Biol. 241, 106–116.

Kacena, M.A., Troiano, N.W., Coady, C.E., Horowitz, M.C., 2003. Decalcification of mounted bone sections enhances immunohistochemical staining. J. Histotechnol. 26, 105–109.

Kiliaridis, S., Engstrom, C., Thilander, B., 1985. The relationship between masticatory function and craniofacial morphology. I. A cephalometric longitudinal analysis in the growing rat fed a soft diet. Eur. J. Orthod. 7, 273–283.

Maes, C., Carmeliet, P., Moermans, K., Stockmans, I., Smets, N., Collen, D., Bouillon, R., Carmeliet, G., 2002. Impaired angiogenesis and endochondral bone formation in mice lacking the vascular endothelial growth factor isoforms VEGF164 and VEGF188. Mech. Dev. 111, 61–73.

Mao, J.J., 2002. Mechanobiology of craniofacial sutures. J. Dent. Res. 81, 810–816.

Mao, J.J., Wang, X., Mooney, M.P., Kopher, R.A., Nudera, J.A., 2003. Strain induced osteogenesis of the craniofacial suture upon controlled delivery of low-frequency cyclic forces. Front. Biosci. 8, A10–A17.

Miller, M.W., Nowakowski, R.S., 1988. Use of bromodeoxyuridine-immunohistochemistry to examine the proliferation, migration and time of origin of cells in the central nervous system. Brain Res. 457, 44–52.

Mitchell, P.J., Wang, C., Tjian, R., 1987. Positive and negative regulation of transcription in vitro: enhancer-binding protein AP-2 is inhibited by SV40 T antigen. Cell 50, 847–861.

Mitchell, P.J., Timmons, P.M., Hebert, J.M., Rigby, P.W., Tjian, R., 1991. Transcription factor AP-2 is expressed in neural crest cell lineages during mouse embryogenesis. Genes Dev. 5, 105–119.

Morgenbesser, S.D., Schreiber-Angus, N., Bidder, M., Mahon, K.A., Overbeek, P.A., Horner, J., DePinho, R.A., 1995. Contrasting roles for c-Myc and L-Myc in the regulation of cellular growth and differentation in vivo. Embo. J. 14, 743–756.

Muenke, M., Schell, U., Hehr, A., Robin, N.H., Losken, H.W., Schinzel, A., Pulleyn, L.J., Rutland, P., Reardon, W., Malcolm, S., et al., 1994. A common mutation in the fibroblast growth factor receptor 1 gene in Pfeiffer syndrome. Nat. Genet. 8, 269–274.

Naumann, A., Dennis, J.E., Awadallah, A., Carrino, D.A., Mansour, J.M., Kastenbauer, E., Caplan, A.I., 2002. Immunochemical and mechanical characterization of cartilage subtypes in rabbit. J. Histochem. Cytochem. 50, 1049–1058.

Nottoli, T., Hagopian-Donaldson, S., Zhang, J., Perkins, A., Williams, T., 1998. AP-2-null cells disrupt morphogenesis of the eye, face, and limbs in chimeric mice. Proc. Natl. Acad. Sci. U. S. A. 95, 13714–13719.

Opperman, L.A., 2000. Cranial sutures as intramembranous bone growth sites. Dev. Dyn. 219, 472–485.

Orestes-Cardoso, S.M., Nefussi, J.R., Hotton, D., Mesbah, M., Orestes-Cardoso, M.D., Robert, B., Berdal, A., 2001. Postnatal Msx1 expression pattern in craniofacial, axial, and appendicular skeleton of transgenic mice from the first week until the second year. Dev. Dyn. 221, 1–13.

Ornitz, D.M., Marie, P.J., 2002. FGF signaling pathways in endochondral and intramembranous bone development and human genetic disease. Genes Dev. 16, 1446–1465.

Papetti, M., Herman, I.M., 2002. Mechanisms of normal and tumor-derived angiogenesis. Am. J. Physiol.: Cell. Physiol. 282, C947–C970.

Persing, J.A., Lettieri, J.T., Cronin, A.J., Wolcott, W.P., Singh, V., Morgan, E., 1991. Craniofacial suture stenosis: morphologic effects. Plast. Reconstr. Surg. 88, 563–571 (discussion 572–573).

Popesko, P., 1992. A colour atlas of the anatomy of small laboratory animals. Wolfe Publishing, London.

Reardon, W., Winter, R.M., Rutland, P., Pulleyn, L.J., Jones, B.M., Malcolm, S., 1994. Mutations in the fibroblast growth factor receptor 2 gene cause Crouzon syndrome. Nat. Genet. 8, 98–103.

Recker, R.R., 1983. Bone Histomorphometry: Techniques and Interpretation. CRC Press, Boca Raton.

Richman, J.M., Tickle, C., 1989. Epithelia are interchangeable between facial primordia of chick embryos and morphogenesis is controlled by the mesenchyme. Dev. Biol. 136, 201–210.

Riddle, R.D., Johnson, R.L., Laufer, E., Tabin, C., 1993. Sonic hedgehog mediates the polarizing activity of the ZPA. Cell 75, 1401–1416.

Ronicke, V., Risau, W., Breier, G., 1996. Characterization of the endothelium-specific murine vascular endothelial growth factor receptor-2 (Flk-1) promoter. Circ. Res. 79, 277–285.

Schneider, R.A., Hu, D., Helms, J.A., 1999. From head to toe: conservation of molecular signals regulating limb and craniofacial morphogenesis. Cell Tissue Res. 296, 103–109.

Schorle, H., Meier, P., Buchert, M., Jaenisch, R., Mitchell, P.J., 1996. Transcription factor AP-2 essential for cranial closure and craniofacial development. Nature 381, 235–238.

Solloway, M.J., Robertson, E.J., 1999. Early embryonic lethality in Bmp5;Bmp7 double mutant mice suggests functional redundancy within the 60A subgroup. Development 126, 1753–1768.

Soriano, P., 1999. Generalized lacZ expression with the ROSA26 Cre reporter strain. Nat. Genet. 21, 70–71.

Tokimasa, C., Kawata, T., Fujita, T., Kaku, M., Kawasoko, S., Kohno, S., Tanne, K., 2000. Effects of insulin-like growth factor-I on nasopremaxillary growth under different masticatory loadings in growing mice. Arch. Oral Biol. 45, 871–878.

Wilkie, A.O., Morriss-Kay, G.M., 2001. Genetics of craniofacial development and malformation. Nat. Rev. Genet. 2, 458–468.

Wilkie, A.O., Slaney, S.F., Oldridge, M., Poole, M.D., Ashworth, G.J., Hockley, A.D., Hayward, R.D., David, D.J., Pulleyn, L.J., Rutland, P., et al., 1995. Apert syndrome results from localized mutations of FGFR2 and is allelic with Crouzon syndrome. Nat. Genet. 9, 165–172.

Wilkinson, D.G., 1992. In Situ Hybridization: A Practical Approach. IRL Press, Oxford.

Williams, T., Tjian, R., 1991a. Analysis of the DNA-binding and activation properties of the human transcription factor AP-2. Genes Dev. 5, 670–682.

Williams, T., Tjian, R., 1991b. Characterization of a dimerization motif in AP-2 and its function in heterologous DNA-binding proteins. Science 251, 1067–1071.

Wysocki, C.J., 1979. Neurobehavioral evidence for the involvement of the vomeronasal system in mammalian reproduction. Neurosci. Biobehav. Rev. 3, 301–341.

Zelzer, E., McLean, W., Ng, Y.S., Fukai, N., Reginato, A.M., Lovejoy, S., D'Amore, P.A., Olsen, B.R., 2002. Skeletal defects in VEGF(120/120) mice reveal multiple roles for VEGF in skeletogenesis. Development 129, 1893–1904.

Zhang, J., Williams, T., 2003. Identification and regulation of tissue-specific cis-acting elements associated with the human AP-2α gene. Dev. Dyn. 228, 194–207.

Zhang, J., Hagopian-Donaldson, S., Serbedzija, G., Elsemore, J., Plehn-Dujowich, D., McMahon, A.P., Flavell, R.A., Williams, T., 1996. Neural tube, skeletal and body wall defects in mice lacking transcription factor AP-2. Nature 381, 238–241.

Zhang, X., Kuroda, S., Carpenter, D., Nishimura, I., Soo, C., Moats, R., Iida, K., Wisner, E., Hu, F.Y., Miao, S., Beanes, S., Dang, C., Vastardis, H., Longaker, M., Tanizawa, K., Kanayama, N., Saito, N., Ting, K., 2002. Craniosynostosis in transgenic mice overexpressing Nell-1. J. Clin. Invest. 110, 861–870.